Bulletin of the Seismological Society of America, Vol. 99, No. 2B, pp. 1103–1131, May 2009, doi: 10.1785/0120080084

An Asymmetric Micropolar Moment Tensor Derived from a Discrete-Block Model for a Rotating Granular Substructure

by Robert J. Twiss

Abstract I define an asymmetric moment tensor for individual slip events and for an average over multiple slip events using a discrete rigid-block model to account for the brittle deformation of a granular material. For the brittle crust, the grains are taken to be fault-bounded blocks. Permanent deformation accumulates by slip events on the boundaries of the blocks. The deformation is described by two independent motions: the local relative motion of the block centroids and the local rigid rotation of the blocks about their centroids. Averaging each of these local motions over multiple slip events in a volume defines both the macrodeformation, which consists of the macrostrain and macrorotation, and the microrotation. An asymmetric local micropolar moment tensor and an asymmetric micropolar moment-density tensor are defined from the local and the averaged motions, respectively.

The model shows (1) the symmetric part of the micropolar moment tensors depends on the constant-volume local shear strain of the block centroids or its averaged equivalent, the macrostrain; (2) the antisymmetric part depends on an objective quantity defined as the difference between the rotational component associated with the centroid deformation and the local block rotation, or their averaged equivalents the macrorotation and the microrotation; and (3) the symmetric and antisymmetric parts of the micropolar moment-density tensor can be inferred up to a scalar magnitude by a micropolar inversion of standard seismic focal mechanisms.

Three field tests show consistency with the theory, but definitive tests are thwarted by insufficient quantitative information or insufficient resolution of the available data.

Introduction

Seismic moment tensors are usually reported as symmetric tensors, even though evidence exists that at least in some cases the tensors have an antisymmetric part (Molnar and Deng, 1984; Sipkin, 1986; Miller *et al.*, 1998). Randall (1971) and Molnar (1983) defined an asymmetric seismic moment tensor for an individual seismic event by an equation nominally similar to the one used in this article. Using the notation in this article, the equation they proposed is essentially

$$m_{kl}^{(\alpha)} = \lambda^{(\alpha)} \nu_k^{(\alpha)} \eta_l^{(\alpha)} S^{(\alpha)}, \tag{1}$$

where for the αth slip event, $m_{kl}^{(\alpha)}$ is the geometric moment tensor, which differs from the standard seismic moment tensor only by the omission of the shear modulus on the right-hand side of the equation; $\lambda^{(\alpha)}$ is the magnitude of the average displacement on the slip surface; $\nu_k^{(\alpha)}$ is the unit vector parallel to the slip direction; $\eta_l^{(\alpha)}$ is the unit normal to the slip surface; and $S^{(\alpha)}$ is the area of the slip surface. Molnar (1983) attempted to relate the antisymmetric part of this moment tensor to the antisymmetric part of the displacement gradient tensor associated with individual seismic events. Kostrov (1974) criticized the definition in equation (1), however, as being physically incorrect because the vectors $\nu_k^{(\alpha)}$ and $\eta_l^{(\alpha)}$ are indistinguishable in the dipole approximation. Jackson and McKenzie (1988) argued, moreover, that the antisymmetric part of this tensor is not independent of the rigid rotation of the coordinate system in which the tensor components are described. It, therefore, does not define an objective tensor and should not be used in an analytical treatment of a physical phenomenon.

Other mechanisms have been proposed as explanations for antisymmetry in the seismic moment tensor, such as heterogeneous slip distribution on a fault (Takeo, 2006), rotational components of motion (see Teisseyre *et al.*, 2006) including seismic events on nonplanar faults, source multiplicity, near-source structural complexity, anisotropy, and tensile failure under high fluid pressure (see references in Sipkin, 1986; Julian *et al.*, 1998). In this article, I propose a model for a granular material by which we can represent the kinematic effect of fault blocks in deforming crust. The model accounts for a rotation of the blocks that is indepen-

dent of the large-scale deformation, and it leads to an objective asymmetric moment tensor.

The recent status of investigations into rotational effects in seismology is provided in this issue of the *Bulletin of the Seismological Society of America* and in a collection of articles edited by Teisseyre *et al.* (2006). Both collections include theoretical developments for materials with substructure, such as granular materials. Such materials can be modeled using the well-established continuum theories of materials with substructure, including the director theories (Cosserat and Cosserat, 1909) and theories of micromorphic and micropolar mechanics (e.g., Eringen, 1966a,b, 1999a,b). These continuum theories are equivalent to assuming that each point in the continuum is attached to a set of three mutually orthogonal unit vectors called directors, which can rotate rigidly and can stretch and shear, independent of the motion of the points to which they are attached.

In both micromorphic and micropolar theories, a large-scale continuum deformation (called the macrodeformation) is defined from the average relative motion of the centroids of the grains in a granular material (Figs. 1 and 2a,b). An independent microdeformation defines the average behavior of the individual grains relative to their centroids, which (in the continuum description) is equivalent to the rotation, stretching, and shearing of the directors. For micropolar materials, the microdeformation is restricted to a rigid rotation of the grains (Fig. 2a,c), which is the model I use in this article; for micromorphic materials the grains can also deform.

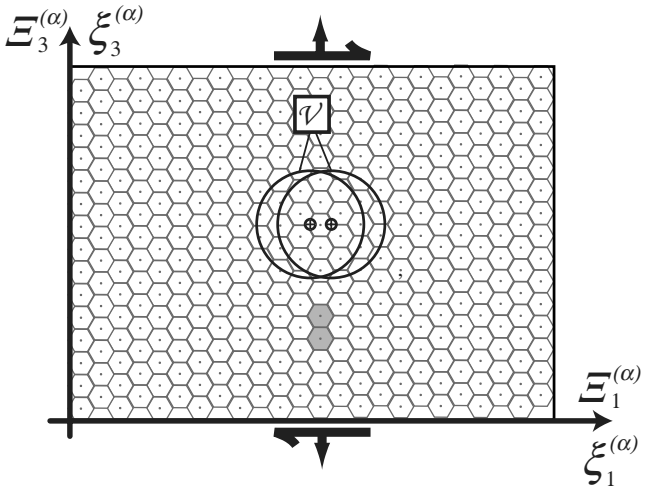

Figure 1. A two-dimensional model of an idealized granular material subjected to a divergent dextral shear. The dots locate the centroids of each hexagonal block. The blocks are rigid so the local deformation occurs at the block boundaries. An average of the components of motion over a continuously movable volume $\mathcal{V}$ defines the values of the continuum field variables at the centroid of the volume $\mathcal{V}$. The average of the block-centroid motions defines the continuum macromotion, and the average of the block rotations about their centroids defines the continuum microrotation. The local deformation for the two shaded blocks is examined in detail in Figure 2.

Seismic events on the surfaces surrounding an individual grain accommodate the relative motion of the grain centroids, the macrodeformation, as well as the independent rotation of the grain, the microrotation. The antisymmetric part of the asymmetric micropolar moment tensor describes the difference between the microrotation and the rotational component of the macrodeformation. Because the difference between two independent rotations is itself independent of the rotation of the reference frame in which the rotations are described, it is objective and, therefore, suitable as a constitutive variable for describing physical phenomena.

A micropolar continuum description of a granular material can be defined by assigning the value of a variable at any given point in the continuum to be the average of that variable over a finite volume $\mathcal{V}$ of the granular material for which the centroid of the volume is at the particular point. $\mathcal{V}$ is large relative to the scale of the grains but is small relative to the scale of the deforming body (Fig. 1). Under these circumstances, the average behavior of the grains becomes represented by the behavior of the directors in the continuum model. The moment arms for the grains are of finite length (as defined by the grain dimensions) and, therefore, torques can accumulate on the grains. In the averaging that leads to the micropolar continuum description, these torques lead to couple stresses and to an antisymmetric component for the stress tensor at each point in the continuum (e.g., Eringen, 1966a,b; Pujol, 2009).

The classical continuum theory assumes the moment of momentum is balanced at each point in the continuum, which leads to a symmetric stress tensor, a double-couple mechanism for seismic events, and thus, a symmetric seismic moment tensor. For a material with a granular substructure, however, the moment of momentum need be balanced only over volumes of finite size, which are defined by the grains of the material substructure, because the torques supported by the rigid grains contribute to the balance of moment of momentum. These torques appear as couple stresses in the micropolar continuum description. Thus, in the block model a seismic event at one surface of a grain can be considered a single-couple event for which the moment of momentum is balanced by torques on the grain.

The substructure of micromorphic materials gives rise to transient seismic rotational waves Teisseyre (1973, 1974) (see also Teisseyre and Boratyński, 2006; Teisseyre and Kozák, 2006). These waves, however, are difficult to detect and leave no permanent deformation. In contrast to studies of such transient effects, I and my colleagues have used the kinematic micropolar theory to investigate the permanent, or nonrecoverable, effects of rotational motions in granular materials during seismogenic deformation (e.g., Twiss *et al.*, 1991, 1993; Unruh *et al.*, 1996; Twiss and Unruh, 1998; Lewis *et al.*, 2007; Twiss and Unruh, 2007).

The effects of a granular substructure on seismic signals become important when the scale of observation of the signal is comparable to the scale of the substructure. In our case, the grains are the fault blocks in the brittlely deforming crust.

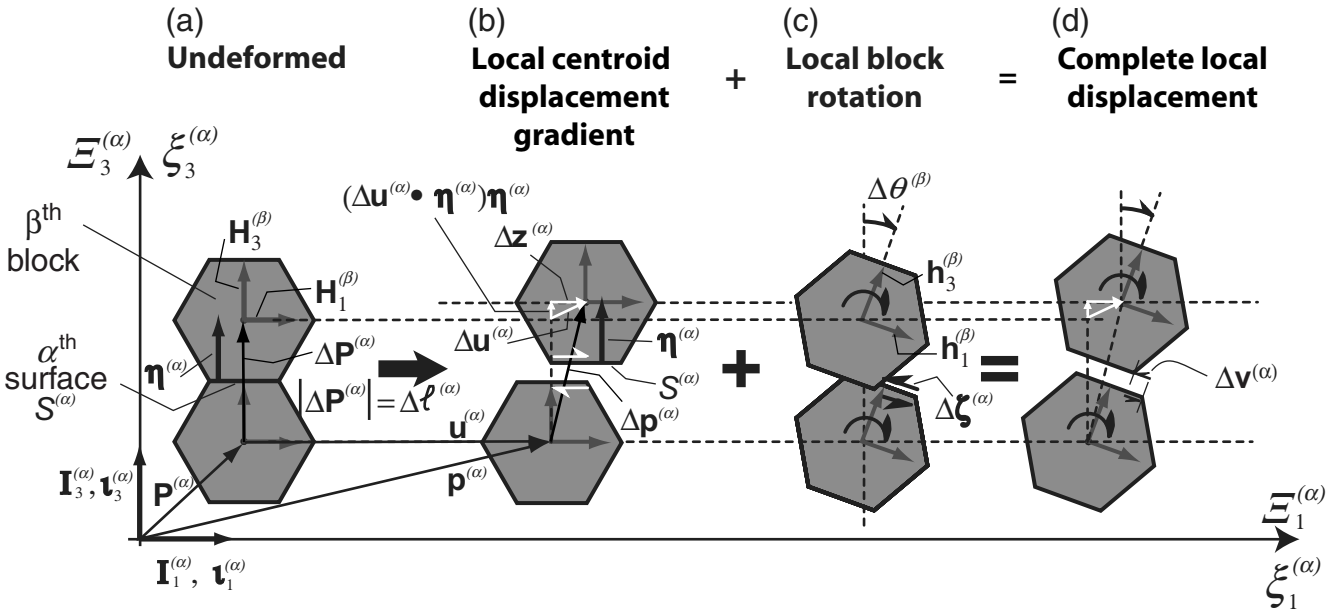

Figure 2. Deformation of a two-dimensional discrete-block model for a granular material, as defined by two representative blocks (shaded blocks in Fig. 1). (After Twiss and Unruh, 1998, fig. 4.) (a) The undeformed state. $\boldsymbol{\eta}^{(\alpha)}$ is the unit normal to the αth surface, and it points into the βth block. $\mathbf{P}^{(\alpha)}$ is the position vector of the centroid of the lower block. $\Delta\mathbf{P}^{(\alpha)}$ is the vector between centroids of neighboring blocks, which has a component of length normal to the αth surface of $\Delta\ell^{(\alpha)}$. $\mathbf{H}_1^{(\beta)}$ and $\mathbf{H}_3^{(\beta)}$ are unit vectors parallel to material lines in the rigid blocks, which therefore rotate with the rigid rotation of the blocks. (b) The deformed state resulting only from the local centroid deformation component: $\mathbf{p}^{(\alpha)}$ and $\mathbf{u}^{(\alpha)}$ are the position vector and the displacement vector, respectively, for the centroid of the lower block. $\Delta\mathbf{p}^{(\alpha)}$ and $\Delta\mathbf{u}^{(\alpha)}$ are the change in the position vector and the displacement vector, respectively, for the centroid of the upper (βth) block relative to that of the lower block. The white arrows $\Delta\mathbf{z}^{(\alpha)}$ and $(\Delta\mathbf{u}^{(\alpha)} \cdot \boldsymbol{\eta}^{(\alpha)})\boldsymbol{\eta}^{(\alpha)}$ are the shear and normal components of the displacement $\Delta\mathbf{u}^{(\alpha)}$ parallel and normal, respectively, to the αth surface. The white shear couple on opposite sides of the αth surface illustrates the shear $\Delta\mathbf{z}^{(\alpha)}$ on the αth surface. (c) The deformed state resulting only from the block-rotation component: $\mathbf{h}_1^{(\beta)}$ and $\mathbf{h}_3^{(\beta)}$ are the unit vectors $\mathbf{H}_1^{(\beta)}$ and $\mathbf{H}_3^{(\beta)}$ after rotation of the block by a clockwise angle of $\Delta\theta^{(\beta)}$, which is a positive rotation about an axis that is positive into the diagram. The black shear couple on the αth surface $\Delta\boldsymbol{\zeta}^{(\alpha)}$ is the shear displacement due to the rotation of the two adjacent blocks. Note that this shear couple has the opposite shear sense from the white shear couple in part (b). (d) The total deformation or the sum of the independent centroid deformation and block rotation: $\Delta\mathbf{v}^{(\alpha)}$ is the net slip vector on the αth surface, which is the sum of the slip components $\Delta\mathbf{z}^{(\alpha)}$ and $\Delta\boldsymbol{\zeta}^{(\alpha)}$ shown in parts (b) and (c), respectively.

Thus, we expect the micropolar theory to be of use in accounting for the observations of seismic phenomena for which the scale of the seismic event (e.g., the rupture radius) is comparable to the scale of the grains (or fault blocks) defining the substructure. In the Analysis section, I use a discrete rigid-block model to describe the deformation of a granular material. With this model I define a local asymmetric micropolar moment tensor for each individual seismic event on a single shear surface (Fig. 2) and a micropolar moment-density tensor for clusters of seismic events contained within a volume $\mathcal{V}$. The latter tensor is the average of the local micropolar moment tensors in the volume $\mathcal{V}$ that is large relative to the rupture radius of any of the included events but small relative to the size of the deforming body (Fig. 1). I show that the symmetric part of the asymmetric micropolar moment tensor is defined by the isochoric (or constant-volume) part of the instantaneous strain tensor, which differs from the deviatoric strain in that the volumetric component of the deformation can be anisotropic (i.e., the volumetric strain can be distributed unequally among the three principal strain axes). This result for the symmetric part of the tensor is similar to the results of Kostrov (1974, equation 3.11).

I also show that the antisymmetric part of the asymmetric micropolar moment tensor reflects the instantaneous average relative rotation between the macrocontinuum and the local rotating fault blocks. This result provides the specific relationship that Twiss *et al.* (1993) claimed must exist on the basis of general symmetry arguments.

Our research over the past 15 years has turned up several instances in which we can test aspects of the micropolar model. In the section Evidence for Nonrecoverable Micropolar Effects, I review evidence from three seismotectonic studies that supports this model.

In the following analysis we refer to the micropolar moment tensor as a shorthand name for the objective asymmetric isochoric micropolar geometric moment tensor. The geometric moment tensor is defined in a manner similar to the standard seismic moment tensor, except that the shear modulus is omitted from the definition. The result is that the geometric moment tensor is related to the deformation of the material rather than to the stress. Ultimately the rela-

tion to the deformation is more appropriate because the deformation is the directly observable quantity, whereas the stress can be only inferred from the deformation and then only by making additional assumptions about the mechanical properties of the material (Twiss and Unruh, 1998). Thus, one can view the classical seismic moment tensor as the geometric moment tensor multiplied by the shear modulus that is introduced simply as a means of expressing the primary description of the deformation in units of stress.

We use the common Einstein summation convention by which summation is implied over repeated subscripts in the same term, and we use the subscript comma notation to indicate partial differentiation with respect to the coordinates x_k, that is, for vector components v_k,

$$v_{k,l} \equiv \frac{\partial v_k}{\partial x_l}. \tag{2}$$

In distinguishing the symmetric and antisymmetric components, with respect to subscripts k and l, of tensors such as t_{kl} and $t_{km}v_{ml}$, we use the shorthand subscript notation:

$$t_{(kl)} \equiv \frac{1}{2}(t_{kl} + t_{lk}), \qquad t_{(km}v_{ml)} \equiv \frac{1}{2}(t_{km}v_{ml} + t_{lm}v_{mk}),$$
$$t_{[kl]} \equiv \frac{1}{2}(t_{kl} - t_{lk}), \qquad t_{[km}v_{ml]} \equiv \frac{1}{2}(t_{km}v_{ml} - t_{lm}v_{mk}). \tag{3}$$

Table 1 gives a list of the symbols used in the analysis, the definition of each, and the equation in which each is first used or defined.

Analysis

In this section, I develop the equations for the asymmetric micropolar moment tensor and illustrate them with reference to the deformation of a geometrically idealized two-dimensional model of a granular material (Figs. 1 and 2). After setting up the basis for the model (see the section The Discrete-Block Model), I derive separately the contributions to the micropolar moment tensor and its volume average, the micropolar moment-density tensor. These tensors are derived, respectively, from the local centroid deformation and from its volume average, the macrodeformation (see the section Local Centroid Deformation Components). I then derive the contributions provided respectively by the local block rotation and its volume average, the microrotation (see the section Local Block-Rotation Components). In each case, I initially derive the local micropolar moment tensor for each slip event in the local coordinates $\xi_k^{(\alpha)}$, as defined in the following section. These coordinates are unique to each of the N slip events, so I then transform the expressions from the local coordinates to the common coordinates x_k so that the results for each slip event can be averaged together. In the section The Complete Micropolar Moment Tensor, for both the local and the volume-averaged cases, I add the separate contributions together to find the expressions for the complete local micropolar moment tensor and the complete micropolar moment-density tensor. Finally, I show how the volume-averaged results for the discrete-block model are related to the results derived by Twiss *et al.* (1991, 1993) for the micropolar continuum theory (see the section Comparison of the Discrete-Block and Continuum Models of Deformation). The present derivation, however, provides additional relations not available from the earlier work. In particular, it shows that the symmetric part of the local moment tensor contains information about the microrotation, which explains how inversion of symmetric focal mechanisms can give information about the microrotation. It also provides a specific relation between the relative vorticity parameter of the continuum micropolar theory and the micropolar moment-density tensor, which previously we had not derived.

The present analysis is done using quantities that describe the instantaneous deformation. These are equivalent to similar quantities that describe the deformation rate. In particular, the instantaneous strain, instantaneous rotation, instantaneous deformation parameter, and instantaneous relative rotation parameter are equivalent, respectively, to the strain rate, rotation rate or vorticity, deformation rate parameter, and relative vorticity parameter of micropolar theory (Twiss *et al.*, 1991, 1993). They differ only by a factor of an infinitesimal increment of time dt, which is an immaterial factor in the analysis.

The Discrete-Block Model

The structure of a granular material is idealized in two dimensions by a set of hexagonal blocks tiling a plane. The deformation is concentrated as discrete slip events on the interfaces between the blocks. These interfaces can be numbered in some unique way, and the interface under consideration is the αth interface (Fig. 2a). In some cases, it is also convenient to consider the blocks to be uniquely numbered and to refer to the βth block (Fig. 2a), with the surfaces of that block numbered $\gamma = 1{:}6$ (see the figure in Appendix A).

The motion of the centroids of the blocks is distinguished from the independent rotation of the blocks about their centroids. These two independent components of the motion are defined at both the local and the volume-averaged scales. For two fault blocks (or grains) in the granular material that are adjacent to each other across an interface (e.g., the gray-shaded blocks in Figs. 1 and 2), I define the local centroid motions and the local block rotations to be the motions that result from a single slip event at an individual interface. Accommodation problems, which are second order effects, are ignored. These motions are also averaged over all the $\alpha = 1{:}N$ slip events in a volume $\mathcal{V}$, where $\mathcal{V}$ is large enough to contain many slip events (empirically, many implies more than about 20 events) but is small relative to the size of the deforming body (Fig. 1). The values of these averages are associated with the point at the centroid of

Table 1

List and Definition of Variables

Symbol	Definition	Equation Number
$\bar{d}_{kl}$, $\hat{\bar{d}}_k$	The macrodeformation rate tensor; symmetric part of the macrovelocity gradient tensor in the continuum micropolar theory; the superposed circumflex and single subscript indicate the principal values.	(103), (125)
e_{kl}, $\hat{e}_{kl}$, $\hat{e}_k$	Volume-averaged macrostrain; symmetric part of the averaged macrodisplacement gradient $u_{k,m}$. Both symbols with a circumflex (hat) are components in the principal coordinates of e_{kl}; the symbol with one subscript are the principal values.	(44), (128)
$\bar{e}_{kl}$, $\hat{\bar{e}}_{kl}$	The macrostrain in the continuum micropolar theory, shown respectively as components in the common reference coordinates x_k, and in the principal coordinates of $\bar{e}_{kl}$.	(104), (117), (127)
$\mathbf{H}_\kappa^{(\beta)}$	An orthogonal triad of material unit vectors in the unrotated βth block, which are rotated with the block into the triad of material unit vectors $\mathbf{h}_\kappa^{(\beta)}$.	Fig. 2a,b; (47)
$\mathbf{h}_\kappa^{(\beta)}$	An orthogonal triad of material unit vectors in the rotated βth block, which have been rotated with the block from the triad of material unit vectors $\mathbf{H}_\kappa^{(\beta)}$ in the unrotated block.	Fig. 2c,d; (47), (48)
$\mathbf{I}_K^{(\alpha)}$	Unit base vectors in the $\Xi_K^{(\alpha)}$ local coordinate system; see $\Xi_K^{(\alpha)}$ for specific orientations.	Fig. 2; (4)
$\mathbf{i}_k$	Base vectors in the common coordinate system x_k, taken for the sake of being specific, to be $\mathbf{i}_1 =$ east, $\mathbf{i}_2 =$ north, $\mathbf{i}_3 =$ up.	(8)
$\bar{L}$	The magnitude of the gradient, normal to the αth shear plane, of the slip velocity from the continuum micropolar theory. It has units of inverse time.	(103)
$\Delta\ell^{(\alpha)}$	The component of the centroid-to-centroid vector $\Delta\mathbf{p}^{(\alpha)}$ in the direction normal to the shear plane. It is a measure of the size of the fault blocks adjacent to the αth shear plane.	(16)
${}_{(d)}M_0^{(\alpha)}$	The local scalar geometric moment for a slip event on the αth surface contributed by the macrodeformation.	(24), (26)
$\bar{M}_0^{(\alpha)}$	The local scalar geometric moment defined for the continuum micropolar theory.	(109)
${}_{(d)}\mathcal{M}_{kl}$	Contribution of the macrodeformation to the micropolar geometric moment-density tensor for a set of slip events in a given volume $\mathcal{V}$.	(36), (37)
${}_{(r)}\mathcal{M}_{ij}$	The part of the micropolar moment-density tensor contributed by the local block rotations for a set of slip events in a volume $\mathcal{V}$.	(66), (67)
$\mathcal{M}_{kl}$, $\mathcal{M}_{kl}^{\mathrm{T}}$, $\hat{\mathcal{M}}_{kl}^{\mathrm{T}}$	The complete micropolar moment-density tensor and its transpose. The circumflex (hat) indicates components in the principal coordinates of e_{kl}.	(92)–(96), (100), (101)–(102), (129)
$\bar{\mathcal{M}}_{kl}$, $\bar{\mathcal{M}}_{kl}^{\mathrm{T}}$	The micropolar moment-density tensor for the continuum micropolar theory and its transpose.	(114)–(115), (122)–(123)
${}_{(d)}\tilde{m}_{kl}^{(\alpha)}$, ${}_{(d)}m_{kl}^{(\alpha)}$	The part of the local micropolar geometric moment tensor contributed by the local centroid deformation. Components are in the local ($\xi_k^{(\alpha)}$) and common (x_k) coordinates systems, respectively.	(24), (27), (33), (34)
${}_{(r)}\tilde{m}_{kl}^{(\alpha)}$, ${}_{(r)}m_{kl}^{(\alpha)}$	The part of the local micropolar moment tensor contributed by the local block rotation. Components are in the local ($\xi_k^{(\alpha)}$) and common (x_k) coordinates systems, respectively.	(62), (65)
$\tilde{m}_{kl}^{(\alpha)}$, $m_{kl}^{(\alpha)}$	The complete local micropolar moment tensor. Components are in the local ($\xi_k^{(\alpha)}$) and common (x_k) coordinates systems, respectively.	(81)–(83), (87)–(90)
$\bar{m}_{kl}^{(\alpha)}$	The local micropolar moment tensor for an individual event defined in the continuum micropolar theory.	(109)
$\Delta\mathbf{P}^{(\alpha)}$	Before a slip event, the relative position of the centroids of the two blocks adjacent to the αth surface.	Fig. 2; (4)
$\Delta\mathbf{p}^{(\alpha)}$	After a slip event, the relative position of the centroids of the two blocks adjacent to the αth surface.	Fig. 2; (6)
$Q_{kl}^{(\alpha)}$	Orthogonal transformation that transforms components in the local $\xi_k^{(\alpha)}$ coordinates to components in the x_k coordinates. It is defined by the dot products of the base vectors $\mathbf{i}_k$ and $\boldsymbol{\iota}_l^{(\alpha)}$.	(8)
$\tilde{\mathfrak{R}}_{kl}^{(\beta)}$	Orthogonal transformation tensor that rotates $\mathbf{H}_\kappa^{(\beta)}$ in the unrotated fault block into $\mathbf{h}_\kappa^{(\beta)}$ in the rotated fault block; the tensor is nonsymmetric. Components written with a superposed tilde are given in the local coordinate system $\xi_k^{(\alpha)}$.	(48), (49), (51)
$\tilde{R}_{kl}^{(\beta)}$, $R_{kl}^{(\beta)}$	The local block-rotation tensor for the βth block; an antisymmetric tensor. Components are in the local ($\xi_k^{(\alpha)}$) and common (x_k) coordinates systems, respectively.	(52), (60)
$\mathcal{R}_{kl}$, $\hat{\mathcal{R}}_{kl}$	The volume-averaged microrotation for a set of N events in a volume $\mathcal{V}$. The circumflex (hat) indicates components in the principal coordinates of e_{kl}.	(68), (128)
$\bar{\mathcal{R}}_{kl}$, $\hat{\bar{\mathcal{R}}}_{kl}$	The microrotation in the continuum micropolar theory, shown as components in the common reference coordinates $x_k$and in the principal coordinates of $\bar{d}_{kl}$, respectively.	(104), (120), (127)
r_{kl}, $\hat{r}_{kl}$	Volume-averaged macrorotation; antisymmetric part of the averaged macrodisplacement gradient $u_{k,m}$. The circumflex (hat) indicates components in the principal coordinates of e_{kl}.	(44), (128)
$\bar{r}_{kl}$, $\hat{\bar{r}}_{kl}$	The macrorotation in the continuum micropolar theory, shown as components in the common reference coordinates x_k and in the principal coordinates of $\bar{e}_{kl}$, respectively.	(104), (119), (127)
$S^{(\alpha)}$	The area of the αth surface.	(1), (26)
$\Delta\mathbf{u}^{(\alpha)}$, $\Delta\tilde{u}_k^{(\alpha)}$	The local displacement of the centroid of one block relative to the centroid of the adjacent block that shares the αth interface and its components in the $\xi_k^{(\alpha)}$ coordinates.	(7), (13)
$\frac{\partial\tilde{u}_k^{(\alpha)}}{\partial\xi_l^{(\alpha)}}$, $u_{k,l}^{(\alpha)}$	Local centroid displacement gradient in the local coordinates $\xi_k^{(\alpha)}$ and the common coordinates x_k. The subscript comma notation ",l" indicates the partial differentiation $\partial u_k^{(\alpha)}/\partial x_l$.	(13), (23)
$u_{k,l}$	Volume-averaged macrodisplacement gradient tensor components given in the common coordinate system. The subscript comma notation ",l" indicates the partial differentiation $\partial u_k/\partial x_l$.	(38)
$u_{k,l}^{(\mathrm{isoc})}$	The volume-averaged isochoric (constant volume) macrodisplacement gradient.	(40), (41)
$\bar{u}_{k,l}$	The macrodisplacement gradient in the continuum micropolar theory.	(105), (116)

(*continued*)

Table 1 (*Continued*)

Symbol	Definition	Equation Number
$V^{(\alpha)}$	The local volume associated with the αth surface over which the shear on the αth surface is considered to be distributed. Same as $V^{(\beta\gamma)}$, but with a different system for labeling the surfaces.	(29)
$V^{(\beta\gamma)}$	The volume associated with the γth surface of the βth block, consisting of portions of the volume of the βth block and of the adjacent block across the γth surface.	Fig. A1; (A3)
$V^{(\beta)}$	Volume of the βth block.	Fig. A1; (A3)
$\mathcal{V}$	A volume that contains a large number N of slip events, where $\mathcal{V}$ is large relative to the rupture radius of any of the events contained within it but is small relative to the scale of the deforming granular material body.	Fig. 1; (35), (36)
$\Delta v^{(\alpha)}$	Scalar magnitude of the complete local slip vector $\Delta\mathbf{v}^{(\alpha)}$ on the αth surface.	(77)
$\Delta\mathbf{v}^{(\alpha)}$, $\Delta\tilde{v}_k^{(\alpha)}$, $\Delta v_k^{(\alpha)}$	The complete local slip vector on the αth surface comprising the sum of the slip components from the local centroid deformation and the local block rotation. Components are in the local ($\xi_k^{(\alpha)}$) and common (x_k) coordinates systems, respectively.	(72), (73), (75)
$\bar{W}_k$	The relative vorticity parameter vector in the continuum micropolar theory.	(125)
$\bar{W}$	The relative vorticity parameter in the continuum micropolar theory. Defined in the principal coordinates of the deformation rate tensor d_{kl} to be $\bar{W}_2$, the second component of the relative vorticity parameter vector.	(126)
$\bar{w}_{lm}$, $\hat{\bar{w}}_{lm}$	The macrospin tensor; antisymmetric part of the macrovelocity gradient tensor in the continuum micropolar theory; the superposed circumflex indicates components in the principal coordinates of the deformation rate tensor d_{kl}.	(103), (125)
x_k	The common coordinate system, taken for the sake of being specific, to be x_1 = east, x_2 = north, x_3 = up. The base vectors in this coordinate system are $\mathbf{i}_k$.	Fig. A1; (8), (9)
$\Delta\mathbf{z}^{(\alpha)}$, $\Delta\tilde{z}_k^{(\alpha)}$, $\Delta z_k^{(\alpha)}$	The contribution to the shear on the αth surface from the local centroid deformation. Components are in the local ($\xi_k^{(\alpha)}$) and common (x_k) coordinates systems, respectively.	(10), (14), (23)
δ_{kl}	Kronecker delta; component = 1 if $k = l$; component = 0 if $k \neq l$.	(8), (18), (A20)
ε_{klm}	Variously called the alternating tensor, the permutation symbol, the antisymmetric symbol, the Eddington epsilon, or the Levi–Civita symbol, it takes values of $+1$ or -1 if $\{klm\}$ is an even or odd permutation of $\{123\}$, respectively, and a value of 0 if any two subscripts are the same.	(50)
Φ_{kl}, $\hat{\Phi}_{kl}$	The anisotropic volumetric macrodeformation tensor. Measure of volumetric deformation that is distributed unequally among the three principal axes of strain. The circumflex (hat) indicates components in the principal coordinates of e_{kl}	(39)
$\bar{\Phi}_{kl}$	The anisotropic volumetric macrodeformation tensor in the continuum micropolar theory. Measure of volumetric deformation that is distributed unequally among the three principal axes of strain.	(118)
$\boldsymbol{\eta}^{(\alpha)}$, $\tilde{\eta}_m^{(\alpha)}$, $\eta_m^{(\alpha)}$	The unit normal to the αth surface. Components are in the local ($\xi_k^{(\alpha)}$) and common (x_k) coordinates systems, respectively.	(11), (23)
$\boldsymbol{\iota}_k^{(\alpha)}$	Unit base vectors in the $\xi_k^{(\alpha)}$ coordinate system; they are parallel to $\mathbf{I}_K^{(\alpha)}$.	Fig. 2; (6), (8)
$\lambda^{(\alpha)}$	The magnitude of the slip vector averaged over the area $S^{(\alpha)}$ of the αth shear plane.	(1)
$\bar{\lambda}^{(\alpha)}$	The magnitude of the slip vector averaged over the area $S^{(\alpha)}$ of the αth shear plane for the continuum micropolar theory.	(109)
$\nu_k^{(\alpha)}$	Components of the unit vector that is parallel to the direction of the complete local slip vector $\Delta\mathbf{v}^{(\alpha)}$ in the αth shear plane.	(77), (78)
$\bar{\boldsymbol{\nu}}^{(\alpha)}$, $\bar{\nu}_m^{(\alpha)}$	The unit vector parallel to the slip velocity vector on the αth shear plane in the continuum micropolar theory and its components in the common x_k coordinate system.	(103), (106)
θ	In the appendices, defines the angle between the unit normals to the surfaces of a block and the common coordinates.	Fig. A1; (A5)
$\Delta\theta^{(\beta)}$	Angle of rotation (microrotation angle) of the βth block about the rotation axis $\boldsymbol{\rho}^{(\beta)}$ through the block centroid. A positive rotation is defined to be a right-handed rotation about the positive rotation axis.	(49), (53)
$\boldsymbol{\rho}^{(\beta)}$, $\tilde{\rho}_k^{(\beta)}$, $\rho_k^{(\alpha)}$	A unit vector through the centroid of the βth block that is parallel to the microrotation axis. Components are in the local ($\xi_k^{(\alpha)}$) and common (x_k) coordinate systems, respectively.	(49), (53), (54), (59)
$\tilde{v}_k^{(\beta)}$	The local microdisplacement field associated with the local block rotation of the βth block about its centroid.	Fig. 3
$\bar{\omega}_{lm}$, $\hat{\bar{\omega}}_{lm}$	The microspin tensor in the continuum analysis; the superposed circumflex indicates components in the principal coordinates of the deformation rate tensor $\bar{d}_{kl}$.	(103), (125)
$\Xi_K^{(\alpha)}$	Local Cartesian coordinate system for the αth surface used to describe the undeformed state. Base vectors in this coordinate system are $\mathbf{I}_K^{(\alpha)}$; $\Xi_3^{(\alpha)}$ and $\mathbf{I}_3^{(\alpha)}$ are normal to the αth interface, and $\Xi_1^{(\alpha)}$ and $\mathbf{I}_1^{(\alpha)}$ are parallel to the total slip direction of the block into which $\mathbf{I}_3^{(\alpha)}$ points.	Figs. 1, 2; (4)
$\Delta\Xi_k^{(\alpha)}$	Components in local coordinates of the relative position vector $\Delta\mathbf{P}^{(\alpha)}$ between the centroids of the two blocks adjacent to the αth slip plane before the slip event.	Fig. 2a; (4)
$\xi_k^{(\alpha)}$	Local Cartesian coordinate system in which the deformed state is described and which has unit base vectors $\boldsymbol{\iota}_k^{(\alpha)}$. We take this coordinate system to be coincident with $\Xi_K^{(\alpha)}$.	Figs. 1, 2
$\Delta\xi_k^{(\alpha)}$	Components in local coordinates of the relative position vector $\Delta\mathbf{p}^{(\alpha)}$ between the centroids of the two blocks adjacent to the αth slip plane after the slip event.	(6), (16)
$\Delta\boldsymbol{\zeta}^{(\alpha)}$, $\Delta\tilde{\zeta}_k^{(\alpha)}$, $\Delta\zeta_k^{(\alpha)}$	The total slip on the αth surface due to the rotation (microrotation) of both blocks on opposite sides of the surface. Components are in the local ($\xi_k^{(\alpha)}$) and common (x_k) coordinates systems, respectively.	(56), (57), (59)

The symbols are listed alphabetically by variable, first for the Roman and then for the Greek alphabets.

$\mathcal{V}$. Because the volume can take any location in space, an average can be defined for any point in the space, thereby defining a micropolar continuum description of the deformation. The average of the local centroid motions defines the continuum macrodeformation, and the average of the local block rotations defines the continuum microrotation. These averaged quantities are equivalent to the macrodeformation and microrotation of the continuum micropolar theory (Twiss *et al.*, 1991, 1993). The local micropolar moment tensor for an individual slip event is defined from the local centroid motion and the local block rotation. The micropolar moment-density tensor is defined from the macrodeformation and the microrotation

The undeformed positions of the block centroids are described in a local Cartesian coordinate system $\Xi_K^{(\alpha)}$, which has unit base vectors $\mathbf{I}_K^{(\alpha)}$ that are perpendicular or parallel to the αth interface (Fig. 2a). $\Xi_3^{(\alpha)}$ and $\mathbf{I}_3^{(\alpha)}$ are normal to the αth interface, and $\Xi_1^{(\alpha)}$ and $\mathbf{I}_1^{(\alpha)}$ are parallel to the complete slip direction on the αth surface. Thus, the ($\Xi_1^{(\alpha)}$, $\Xi_2^{(\alpha)}$) plane is the local shear plane, which contains the slip vector, and the ($\Xi_1^{(\alpha)}$, $\Xi_3^{(\alpha)}$) plane is normal to the shear plane and also contains the slip vector.

Before deformation the relative position of the centroids of the two blocks in contact across the αth surface is given by the vector (Figs. 1 and 2a)

$$\Delta\mathbf{P}^{(\alpha)} = \Delta\Xi_K^{(\alpha)}\mathbf{I}_K^{(\alpha)}. \tag{4}$$

For the particular geometry shown in Figure 2a,

$$\Delta\mathbf{P}^{(\alpha)} = \Delta\Xi_3^{(\alpha)}\mathbf{I}_3^{(\alpha)}. \tag{5}$$

During a slip event the block centroids are displaced relative to one another, and this displacement defines the local centroid motion; the blocks also rotate about their centroids, which defines the independent local block rotation. After a slip event, the geometry of the blocks is described in a coordinate system $\xi_k^{(\alpha)}$, which has unit base vectors $\boldsymbol{\iota}_k^{(\alpha)}$. This coordinate system is taken to be coincident with $\Xi_K^{(\alpha)}$ (Figs. 1 and 2).

The relative position of the two block centroids after the slip event is given by (Fig. 2b)

$$\Delta\mathbf{p}^{(\alpha)} = \Delta\xi_k^{(\alpha)}\boldsymbol{\iota}_k^{(\alpha)}, \tag{6}$$

and the local displacement of one centroid relative to the other is, therefore,

$$\Delta\mathbf{u}^{(\alpha)} \equiv \Delta\mathbf{p}^{(\alpha)} - \Delta\mathbf{P}^{(\alpha)} \tag{7}$$

(Fig. 1b).

The local block rotation of the βth block $\Delta\theta^{(\beta)}$ is a positive rotation if it is a right-handed rotation about the $\xi_2^{(\alpha)}$ coordinate axis, which is positive into the plane of the diagram in Figure 2c; thus, for the axis orientations depicted in Figure 2c, a positive rotation is a clockwise rotation.

It is clear from Figure 2c that a positive increment of rotation of the blocks about the $\xi_2^{(\alpha)}$ axis results in a slip on the αth surface, which is opposite in shear sense to the slip resulting from a positive increment of the local centroid displacement. The complete slip vector is the sum of the shear components contributed by the local centroid displacement and the local block rotation. In general, the complete slip vector is not colinear with either of these shear components because the local centroid displacement need not be in the ($\xi_1^{(\alpha)}$, $\xi_3^{(\alpha)}$) plane and the local block rotation need not be about the $\xi_2^{(\alpha)}$ axis.

We can assume, for the sake of being specific, that the common coordinates consist of the right-handed Cartesian geographic coordinates x_1 = east, x_2 = north, and x_3 = up. The unit base vectors in this coordinate system are $\mathbf{i}_k$. The orthogonal transformation that transforms components in the local coordinates $\xi_k^{(\alpha)}$ to the common coordinates x_k is defined by

$$\begin{gathered} Q_{kl}^{(\alpha)} \equiv \mathbf{i}_k \cdot \boldsymbol{\iota}_l^{(\alpha)} = \cos(\mathbf{i}_k \angle \boldsymbol{\iota}_l^{(\alpha)}), \qquad Q_{kl}^{(\alpha)} Q_{km}^{(\alpha)} = \delta_{lm}, \\ Q_{lk}^{(\alpha)} Q_{mk}^{(\alpha)} = \delta_{lm}, \qquad \det Q_{kl}^{(\alpha)} = 1. \end{gathered} \tag{8}$$

The δ_{lm} are Kronecker deltas. The last constraint on the value of the determinant in equation (8) limits the orthogonal transformations to proper rotations (i.e., reflections are not permitted). A superposed tilde on vector and tensor components indicates they are given in the local coordinates $\xi_k^{(\alpha)}$. Thus, for an arbitrary vector $v_k^{(\alpha)}$ and an arbitrary second rank tensor $t_{kl}^{(\alpha)}$, the components in geographic and local coordinates are related to one another by

$$\begin{gathered} v_i^{(\alpha)} = Q_{ik}^{(\alpha)} \tilde{v}_k^{(\alpha)}, \qquad \tilde{v}_k^{(\alpha)} = v_i^{(\alpha)} Q_{ik}^{(\alpha)}, \\ t_{ij}^{(\alpha)} = Q_{ik}^{(\alpha)} Q_{jl}^{(\alpha)} \tilde{t}_{kl}^{(\alpha)}, \qquad \tilde{t}_{kl}^{(\alpha)} = t_{ij}^{(\alpha)} Q_{ik}^{(\alpha)} Q_{jl}^{(\alpha)}. \end{gathered} \tag{9}$$

Local Centroid Deformation Components

Contribution of the Local Centroid Deformation to the Slip Vector. The contribution to the shear on the surface $S^{(\alpha)}$ from the local centroid motions is the partial slip vector denoted $\Delta\mathbf{z}^{(\alpha)}$ and given by

$$\Delta\mathbf{z}^{(\alpha)} = \boldsymbol{\eta}^{(\alpha)} \times \Delta\mathbf{u}^{(\alpha)} \times \boldsymbol{\eta}^{(\alpha)}, \tag{10}$$

where $\boldsymbol{\eta}^{(\alpha)}$ is the unit normal to the αth surface, $\Delta\mathbf{u}^{(\alpha)}$ is the relative displacement of the centroids of adjacent blocks (equation 7, Fig. 2b), and the multiplication symbol indicates the vector or cross product. By definition,

$$\begin{gathered} \boldsymbol{\eta}^{(\alpha)} \cdot \boldsymbol{\eta}^{(\alpha)} = 1, \qquad \boldsymbol{\eta}^{(\alpha)} = \boldsymbol{\iota}_3^{(\alpha)}, \\ \tilde{\eta}_m^{(\alpha)} = \boldsymbol{\eta}^{(\alpha)} \cdot \boldsymbol{\iota}_m, \qquad \tilde{\eta}_m^{(\alpha)} = [\,0 \quad 0 \quad 1\,], \end{gathered} \tag{11}$$

where the dot indicates the scalar or dot product. It is not difficult to show that (Fig. 2b)

$$\boldsymbol{\eta}^{(\alpha)} \times \Delta\mathbf{u}^{(\alpha)} \times \boldsymbol{\eta}^{(\alpha)} = \Delta\mathbf{u}^{(\alpha)} - (\Delta\mathbf{u}^{(\alpha)} \cdot \boldsymbol{\eta}^{(\alpha)})\boldsymbol{\eta}^{(\alpha)}. \quad (12)$$

The local centroid displacement gradient is defined as the relative displacement of the block centroids for the blocks adjacent to the αth surface, divided by the distance between the centroids (Fig. 2b). Thus, we can express the displacement increment $\Delta\mathbf{u}^{(\alpha)}$ in terms of this local centroid displacement gradient. Using component notation, we write

$$\Delta\tilde{u}_k^{(\alpha)} \equiv \frac{\partial\tilde{u}_k^{(\alpha)}}{\partial\xi_m^{(\alpha)}}\Delta\xi_m^{(\alpha)}. \quad (13)$$

Combining equations (10) and (12), writing the vectors as components in the local coordinate system $\xi_k^{(\alpha)}$, and introducing equation (13) gives

$$\Delta\tilde{z}_k^{(\alpha)} = \left[\frac{\partial\tilde{u}_k^{(\alpha)}}{\partial\xi_m^{(\alpha)}} - \left(\frac{\partial\tilde{u}_j^{(\alpha)}}{\partial\xi_m^{(\alpha)}}\tilde{\eta}_j^{(\alpha)}\tilde{\eta}_k^{(\alpha)}\right)\right]\Delta\xi_m^{(\alpha)}. \quad (14)$$

At the αth surface, the only nonzero components of the local centroid displacement gradient are the gradients along the direction $\boldsymbol{\iota}_3^{(\alpha)}$, that is, $\partial\tilde{u}_k^{(\alpha)}/\partial\xi_3^{(\alpha)}$,

$$\frac{\partial\tilde{u}_k^{(\alpha)}}{\partial\xi_l^{(\alpha)}} = \begin{bmatrix} 0 & 0 & \frac{\partial\tilde{u}_1^{(\alpha)}}{\partial\xi_3^{(\alpha)}} \\ 0 & 0 & \frac{\partial\tilde{u}_2^{(\alpha)}}{\partial\xi_3^{(\alpha)}} \\ 0 & 0 & \frac{\partial\tilde{u}_3^{(\alpha)}}{\partial\xi_3^{(\alpha)}} \end{bmatrix}. \quad (15)$$

From equation (6), we have

$$\Delta\xi_k^{(\alpha)} = \Delta\mathbf{p}^{(\alpha)} \cdot \boldsymbol{\iota}_k^{(\alpha)}, \qquad \Delta\xi_3^{(\alpha)} = \Delta\mathbf{p}^{(\alpha)} \cdot \boldsymbol{\iota}_3^{(\alpha)} \equiv \Delta\ell^{(\alpha)}, \quad (16)$$

whereby for the terms in equation (14), we have

$$\frac{\partial\tilde{u}_k^{(\alpha)}}{\partial\xi_m^{(\alpha)}}\Delta\xi_m^{(\alpha)} = \frac{\partial\tilde{u}_k^{(\alpha)}}{\partial\xi_3^{(\alpha)}}\Delta\xi_3^{(\alpha)} = \frac{\partial\tilde{u}_k^{(\alpha)}}{\partial\xi_m^{(\alpha)}}\tilde{\eta}_m^{(\alpha)}\Delta\ell^{(\alpha)}, \quad (17)$$

where $\tilde{\eta}_m^{(\alpha)}$ is given by the fourth part of equation (11) and $\Delta\ell^{(\alpha)}$ is the component of the centroid-to-centroid vector $\Delta\mathbf{p}^{(\alpha)}$ in the direction normal to the shear plane (Fig. 2b, equation 6). Thus, it is a measure of the block size.

Using equation (17) in equation (14), we have

$$\Delta\tilde{z}_k^{(\alpha)} = \left\{\frac{\partial\tilde{u}_k^{(\alpha)}}{\partial\xi_m^{(\alpha)}} - \left[\frac{\partial\tilde{u}_i^{(\alpha)}}{\partial\xi_j^{(\alpha)}}\tilde{\eta}_i^{(\alpha)}\tilde{\eta}_j^{(\alpha)}\right]\delta_{km}\right\}\tilde{\eta}_m^{(\alpha)}\Delta\ell^{(\alpha)}, \quad (18)$$

where δ_{km} is the Kronecker delta.

Because of the fourth part of equation (11), the only values of equation (18) that can be nonzero are those for which the subscript $m = 3$, and the only nonzero values for the term in square brackets are those for which subscripts $i = j = 3$. Thus, we can write equation (18) as

$$\Delta\tilde{z}_k^{(\alpha)} = \left[\frac{\partial\tilde{u}_k^{(\alpha)}}{\partial\xi_3^{(\alpha)}} - \frac{\partial\tilde{u}_3^{(\alpha)}}{\partial\xi_3^{(\alpha)}}\delta_{k3}\right]\Delta\ell^{(\alpha)}, \quad (19)$$

whereby we find, for the components of the partial slip vector,

$$\Delta\tilde{z}_k^{(\alpha)} = \left\{\begin{bmatrix} \frac{\partial\tilde{u}_1^{(\alpha)}}{\partial\xi_3^{(\alpha)}} & \frac{\partial\tilde{u}_2^{(\alpha)}}{\partial\xi_3^{(\alpha)}} & \frac{\partial\tilde{u}_3^{(\alpha)}}{\partial\xi_3^{(\alpha)}} \end{bmatrix} - \begin{bmatrix} 0 & 0 & \frac{\partial\tilde{u}_3^{(\alpha)}}{\partial\xi_3^{(\alpha)}} \end{bmatrix}\right\}\Delta\ell^{(\alpha)}, \quad (20)$$

$$\Delta\tilde{z}_k^{(\alpha)} = \begin{bmatrix} \frac{\partial\tilde{u}_1^{(\alpha)}}{\partial\xi_3^{(\alpha)}} & \frac{\partial\tilde{u}_2^{(\alpha)}}{\partial\xi_3^{(\alpha)}} & 0 \end{bmatrix}\Delta\ell^{(\alpha)}. \quad (21)$$

The second terms in equations (18) and (20) represent the part of the centroid displacement gradient that is normal to the αth surface; these terms, therefore, describe a uniaxial volumetric deformation. Thus, the slip vector, which lies strictly within the αth surface, is determined by the constant-volume component of the local centroid displacement gradient (Fig. 2b).

For the special case in Figure 2, for which $u_2 = 0$, the components of the partial slip vector on the αth surface are, from equation (21),

$$\Delta\tilde{z}_k^{(\alpha)} = \begin{bmatrix} \frac{\partial\tilde{u}_1^{(\alpha)}}{\partial\xi_3^{(\alpha)}} & 0 & 0 \end{bmatrix}\Delta\ell^{(\alpha)}. \quad (22)$$

We can express the partial slip vector in terms of its components in the common coordinate system x_k by using equations of the type in equation (9). We substitute these forms into equation (18) to change the components in the local coordinate system into the components in the common coordinates. Then, simplifying using equation (8) gives

$$\Delta z_k^{(\alpha)} = [u_{k,m}^{(\alpha)} - (u_{i,j}^{(\alpha)}\eta_i^{(\alpha)}\eta_j^{(\alpha)})\delta_{km}]\eta_m^{(\alpha)}\Delta\ell^{(\alpha)}. \quad (23)$$

The term in parentheses (…), when multiplied by $\Delta\ell^{(\alpha)}$, is just the uniaxial volumetric deformation at each fault surface written in the common coordinates. Therefore, the term in brackets […], when multiplied by $\Delta\ell^{(\alpha)}$, is the constant-volume component of the local centroid displacement gradient written in the common coordinates.

Contribution of the Local Centroid Deformation to the Local Micropolar Moment Tensor. The contribution of the local centroid deformation to the local micropolar moment tensor is written ${}_{(d)}\tilde{m}_{kl}^{(\alpha)}$, where the left subscript (d) identifies the centroid deformation contribution. It is defined to be the product of the local scalar geometric moment contributed by the local centroid deformation ${}_{(d)}M_0^{(\alpha)}$ times the two unit vectors parallel, respectively, to the slip direction and the normal to the slip surface:

$${}_{(d)}\tilde{m}_{kl}^{(\alpha)} = {}_{(d)}M_0^{(\alpha)}\frac{\Delta\tilde{z}_k^{(\alpha)}}{|\Delta\mathbf{z}^{(\alpha)}|}\tilde{\eta}_l^{(\alpha)}, \quad (24)$$

where $|\Delta\mathbf{z}^{(\alpha)}|$ is the magnitude of the slip on the αth slip surface contributed by the local centroid deformation,

$$|\Delta\mathbf{z}^{(\alpha)}| \equiv [\Delta\mathbf{z}^{(\alpha)} \cdot \Delta\mathbf{z}^{(\alpha)}]^{1/2}. \tag{25}$$

The local scalar geometric moment is defined by

$${}_{(d)}M_0^{(\alpha)} = |\Delta\mathbf{z}^{(\alpha)}|S^{(\alpha)}, \tag{26}$$

where $S^{(\alpha)}$ is the area of the αth surface, whereby equation (24) becomes

$${}_{(d)}\tilde{m}_{kl}^{(\alpha)} = \Delta\tilde{z}_k^{(\alpha)}\tilde{\eta}_l^{(\alpha)}S^{(\alpha)}. \tag{27}$$

Using equation (18) in (27) gives

$${}_{(d)}\tilde{m}_{kl}^{(\alpha)} = \left\{\frac{\partial\tilde{u}_k^{(\alpha)}}{\partial\xi_m^{(\alpha)}} - \left[\frac{\partial\tilde{u}_i^{(\alpha)}}{\partial\xi_j^{(\alpha)}}\tilde{\eta}_i^{(\alpha)}\tilde{\eta}_j^{(\alpha)}\right]\delta_{km}\right\}\tilde{\eta}_m^{(\alpha)}\tilde{\eta}_l^{(\alpha)}V^{(\alpha)}, \tag{28}$$

where we have introduced the definition of the volume associated with each plane $S^{(\alpha)}$ by (Fig. 2b),

$$V^{(\alpha)} \equiv \Delta\ell^{(\alpha)}S^{(\alpha)}. \tag{29}$$

Using the fourth part of equation (11), we can expand the expressions in equation (28) to find

$${}_{(d)}\tilde{m}_{kl}^{(\alpha)} = \left\{\begin{bmatrix} 0 & 0 & \frac{\partial\tilde{u}_1^{(\alpha)}}{\partial\xi_3^{(\alpha)}} \\ 0 & 0 & \frac{\partial\tilde{u}_2^{(\alpha)}}{\partial\xi_3^{(\alpha)}} \\ 0 & 0 & \frac{\partial\tilde{u}_3^{(\alpha)}}{\partial\xi_3^{(\alpha)}} \end{bmatrix} - \begin{bmatrix} 0 & 0 & 0 \\ 0 & 0 & 0 \\ 0 & 0 & \frac{\partial\tilde{u}_3^{(\alpha)}}{\partial\xi_3^{(\alpha)}} \end{bmatrix}\right\}V^{(\alpha)}, \tag{30}$$

$${}_{(d)}\tilde{m}_{kl}^{(\alpha)} = \begin{bmatrix} 0 & 0 & \frac{\partial\tilde{u}_1^{(\alpha)}}{\partial\xi_3^{(\alpha)}} \\ 0 & 0 & \frac{\partial\tilde{u}_2^{(\alpha)}}{\partial\xi_3^{(\alpha)}} \\ 0 & 0 & 0 \end{bmatrix}V^{(\alpha)}. \tag{31}$$

Thus, the moment tensor describes only the constant-volume component of the local centroid deformation.

Equation (31) shows that, for an individual slip event such as the one depicted in Figure 2b, the contribution of the local centroid deformation to the local micropolar moment tensor is asymmetric. The existence of an antisymmetric part to this tensor derives ultimately from the fact that, in materials with a granular substructure, the moment of momentum is balanced on the scale of the rigid grains or blocks, not locally at each seismic event as in classical theory. Thus, in defining the micropolar moment tensor we consider only a single-couple mechanism rather than the usual double-couple mechanism that results in a symmetric moment tensor.

For the special case model in Figure 2b, for which $\tilde{u}_2^{(\alpha)} = 0$, equation (31) becomes

$${}_{(d)}\tilde{m}_{kl}^{(\alpha)} = \begin{bmatrix} 0 & 0 & \frac{\partial\tilde{u}_1^{(\alpha)}}{\partial\xi_3^{(\alpha)}} \\ 0 & 0 & 0 \\ 0 & 0 & 0 \end{bmatrix}V^{(\alpha)}. \tag{32}$$

We now transform the components of this part of the local micropolar moment tensor, which are contributed by the local centroid deformation for an individual slip event, to the common geographic coordinate system. Using equation (28), we introduce the transformations in equation (9) and use equation (8) to find

$${}_{(d)}m_{kl}^{(\alpha)} = [u_{k,m}^{(\alpha)} - (u_{i,j}^{(\alpha)}\eta_i^{(\alpha)}\eta_j^{(\alpha)})\delta_{km}]\eta_m^{(\alpha)}\eta_l^{(\alpha)}V^{(\alpha)}. \tag{33}$$

We can obtain the same result by writing the local moment tensor in common coordinates as

$${}_{(d)}m_{kl}^{(\alpha)} = \Delta z_k^{(\alpha)}\eta_l^{(\alpha)}S^{(\alpha)}. \tag{34}$$

Introducing equations (23) and (29) gives equation (33).

Contribution of the Macrodeformation to the Micropolar Moment-Density Tensor. To obtain the contribution of the local centroid deformation to the micropolar moment-density tensor, we must take the average over the volume $\mathcal{V}$ of the contributions from all the N events contained within $\mathcal{V}$ (equation 33), where $\mathcal{V}$ is large relative to the rupture radius of the largest event contained within it but is small relative to the scale of the deforming granular material body (Fig. 1). We must have, therefore,

$$\mathcal{V} \gg V^{(\alpha)} = \Delta\ell^{(\alpha)}S^{(\alpha)}, \tag{35}$$

where the right-hand side of the equation is from equation (29). Thus, the part of the micropolar moment-density tensor contributed by the local centroid deformation is

$${}_{(d)}\mathcal{M}_{kl} \equiv \frac{1}{\mathcal{V}}\sum_{\alpha=1}^{N}{}_{(d)}m_{kl}^{(\alpha)}. \tag{36}$$

Introducing equation (33) gives

$${}_{(d)}\mathcal{M}_{kl} \equiv \frac{1}{\mathcal{V}}\sum_{\alpha=1}^{N}\{u_{k,m}^{(\alpha)} - [u_{i,j}^{(\alpha)}\eta_i^{(\alpha)}\eta_j^{(\alpha)}]\delta_{km}\}\eta_m^{(\alpha)}\eta_l^{(\alpha)}V^{(\alpha)}. \tag{37}$$

We define the macrodisplacement gradient and the anisotropic volumetric macrodeformation tensor to be the average of local centroid displacement gradients at all the slip surfaces $\alpha = 1{:}N$:

$$u_{k,l} \equiv \frac{1}{\mathcal{V}} \sum_{\alpha=1}^{N} u_{k,m}^{(\alpha)} \eta_m^{(\alpha)} \eta_l^{(\alpha)} V^{(\alpha)}, \tag{38}$$

$$\Phi_{kl} \equiv \frac{1}{\mathcal{V}} \sum_{\alpha=1}^{N} [u_{i,j}^{(\alpha)} \eta_i^{(\alpha)} \eta_j^{(\alpha)}] \eta_k^{(\alpha)} \eta_l^{(\alpha)} V^{(\alpha)} = \Phi_{lk}. \tag{39}$$

Equation (39) for the anisotropic volumetric strain accounts for the possibility that the amount of volumetric strain may be different along the different principal strain axes. Such a difference could arise if the normal component of displacement across the shear planes varies with the orientation of the shear plane or if the shear planes have a preferred orientation or both. We define a constant-volume deformation, which we refer to as the isochoric macrodisplacement gradient, by

$$u_{k,l}^{(\mathrm{isoc})} \equiv \frac{1}{\mathcal{V}} \sum_{\alpha=1}^{N} \{u_{k,m}^{(\alpha)} - [u_{i,j}^{(\alpha)} \eta_i^{(\alpha)} \eta_j^{(\alpha)}] \delta_{km}\} \eta_m^{(\alpha)} \eta_l^{(\alpha)} V^{(\alpha)}. \tag{40}$$

Using equations (38) and (39) in equation (40) gives

$$u_{k,l}^{(\mathrm{isoc})} = u_{k,l} - \Phi_{kl}. \tag{41}$$

The definition in equation (39) describes an anisotropic volume change, which in general is unequally distributed among the principal axes of strain. The isochoric macrodisplacement gradient defined in equations (40) and (41), therefore, is not the same as the deviatoric macrodisplacement gradient, which is defined by subtracting an isotropic measure of the volumetric deformation from the macrodisplacement gradient

$$u_{k,l}^{(\mathrm{dev})} \equiv u_{k,l} - \frac{1}{3} u_{i,j} \delta_{ij} \delta_{kl}. \tag{42}$$

Clearly, the isochoric macrodisplacement gradient tensor is the same as the deviatoric macrodisplacement gradient tensor for the special case of isotropic volumetric deformation.

The first scalar invariant for both $u_{k,l}$ and Φ_{kl} defines the total averaged volumetric deformation within the volume $\mathcal{V}$; therefore, this invariant for these two tensors must be equal. Multiplying both sides of equations (38) and (39) by the Kronecker delta δ_{kl} and using equation (11) in the latter, it is easy to show that $\Phi_{kk} = u_{k,k}$ as required.

From equations (40) and (41), we find

$${}_{(d)}\mathcal{M}_{kl} = u_{k,l}^{(\mathrm{isoc})} = u_{k,l} - \Phi_{kl}. \tag{43}$$

Thus, only the isochoric macrodeformation contributes to the micropolar moment-density tensor ${}_{(d)}\mathcal{M}_{kl}$.

We can write this part of the micropolar moment-density tensor in terms of the symmetric average macrostrain e_{kl} and antisymmetric average macrorotation r_{kl} by defining

$$e_{kl} \equiv \frac{1}{2}(u_{k,l} + u_{l,k}) = e_{lk}, \qquad r_{kl} \equiv \frac{1}{2}(u_{k,l} - u_{l,k}) = -r_{lk}, \tag{44}$$

$$u_{k,l} = u_{(k,l)} + u_{[k,l]} = e_{kl} + r_{kl}, \tag{45}$$

where we used the notation defined in equation (3). Equation (43) can then be written

$${}_{(d)}\mathcal{M}_{kl} = e_{kl} - \Phi_{kl} + r_{kl}. \tag{46}$$

The symmetric part of equation (46) is similar to the result derived by Kostrov (1974, equation 3.11), except that Kostrov's equation does not explicitly subtract out the anisotropic volumetric component of the deformation, although that restriction is implicit in his derivation.

Local Block-Rotation Components

Contribution of the Local Block Rotation to the Slip Vector. We now turn our attention to the component of partial slip $\Delta\boldsymbol{\zeta}^{(\alpha)}$ on $S^{(\alpha)}$ that is provided by the local block rotation. We assume that the αth surface is a surface on the βth block so that the surface rotates with the block by an angle $\Delta\theta^{(\beta)}$ about an axis through the centroid of the block. The orientation of the rotation axis is defined by the unit vector $\boldsymbol{\rho}^{(\beta)}$. For the special case in Figure 2c $\boldsymbol{\rho}^{(\beta)} = \boldsymbol{\iota}_2$. An orthogonal triad of material unit vectors in the unrotated βth block $\mathbf{H}_\kappa^{(\beta)}$ (gray lines in the blocks in Fig. 2a) is rotated with the block into the orthogonal triad of material unit vectors $\mathbf{h}_\kappa^{(\beta)}$ in the rotated block (gray lines in the blocks in Fig. 2c), where

$$\begin{aligned} \tilde{H}_{\kappa K}^{(\beta)} \tilde{H}_{\kappa L}^{(\beta)} &= \delta_{KL}, \qquad & \tilde{H}_{\kappa K}^{(\beta)} \tilde{H}_{\lambda K}^{(\beta)} &= \delta_{\kappa\lambda}, \\ \tilde{h}_{\kappa k}^{(\beta)} \tilde{h}_{\kappa l}^{(\beta)} &= \delta_{kl}, \qquad & \tilde{h}_{\kappa k}^{(\beta)} \tilde{h}_{\lambda k}^{(\beta)} &= \delta_{\kappa\lambda}, \end{aligned} \tag{47}$$

and where the deltas are all Kronecker deltas. The rotation tensor for this local block rotation can be written as (see Truesdell and Toupin, 1960, equations 37.1 and 37.2)

$$\tilde{\Re}_{km}^{(\beta)} = \tilde{h}_{\kappa k}^{(\beta)} \tilde{H}_{\kappa M}^{(\beta)} \delta_{Mm}, \qquad \tilde{h}_{\kappa k}^{(\beta)} = \tilde{\Re}_{km}^{(\beta)} \tilde{H}_{\kappa M}^{(\beta)} \delta_{mM}, \tag{48}$$

where for the coincident Cartesian coordinates that we employ, the deltas are Kronecker deltas. This local rotation tensor $\tilde{\Re}_{km}^{(\beta)}$ can be expressed in terms of the rotation angle $\Delta\theta^{(\beta)}$ about a unique unit vector $\boldsymbol{\rho}^{(\beta)}$ parallel to the rotation axis through the centroid of the βth block (see Truesdell and Toupin, 1960, p. 280 and equation 37.17). $\Delta\theta^{(\beta)}$ is determined up to a convention of sign and quadrant, and $\boldsymbol{\rho}^{(\beta)}$ is determined up to the sign of the axis.

$$\begin{aligned} \tilde{\Re}_{km}^{(\beta)} = \tilde{\rho}_k^{(\beta)} \tilde{\rho}_m^{(\beta)} [1 - \cos\Delta\theta^{(\beta)}] + \varepsilon_{mkn} \tilde{\rho}_n^{(\beta)} \sin\Delta\theta^{(\beta)} \\ + \cos\Delta\theta^{(\beta)} \delta_{km}, \end{aligned} \tag{49}$$

where

$$\varepsilon_{mkn} \equiv \boldsymbol{\iota}_m^{(\alpha)} \times \boldsymbol{\iota}_k^{(\alpha)} \cdot \boldsymbol{\iota}_n^{(\alpha)} \tag{50}$$

is variously called the alternating tensor, the permutation symbol, the antisymmetric symbol, the Eddington epsilon, or the Levi–Civita symbol; it takes values of $+1$ or -1 if the subscripts $\{mkn\}$ are, respectively, an even or odd permutation of $\{123\}$, and it takes a value of zero if any two subscripts are the same. We assume $\Delta\theta^{(\beta)}$ is positive if it is a right-handed rotation about the positive direction of $\boldsymbol{\rho}^{(\beta)}$, and the order of subscripts on the alternating tensor in equation (49) ensures that the component $\tilde{\mathfrak{R}}_{13}^{(\beta)}$ (and $\tilde{R}_{13}^{(\beta)}$ defined in equation 52) describes a positive right-handed rotation about the $\xi_2^{(\alpha)}$ axis, as we illustrate in Figure 3 and in the text following equation (55).

If $\Delta\theta^{(\beta)}$ is very small then equation (49) becomes

$$\tilde{\mathfrak{R}}_{km}^{(\beta)} = \varepsilon_{mkn}\tilde{\rho}_n^{(\beta)}\Delta\theta^{(\beta)} + \delta_{km} \quad \text{if } \Delta\theta^{(\beta)} \ll 1 \text{ radian} \tag{51}$$

because $\cos\Delta\theta^{(\beta)} \approx 1$ and $\sin\Delta\theta^{(\beta)} \approx \Delta\theta^{(\beta)}$ (radians).

We define the local instantaneous block-rotation tensor by

$$\tilde{R}_{km}^{(\beta)} \equiv \tilde{\mathfrak{R}}_{km}^{(\beta)} - \delta_{km} = \varepsilon_{mkn}\tilde{\rho}_n^{(\beta)}\Delta\theta^{(\beta)} = -\tilde{R}_{mk}^{(\beta)}, \tag{52}$$

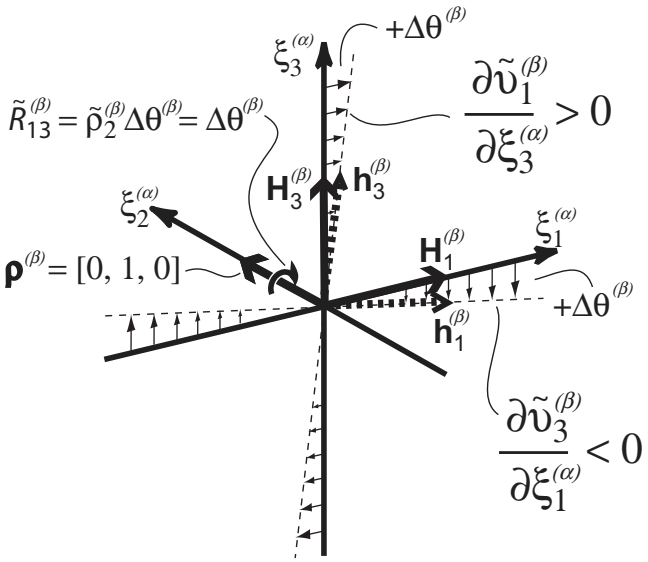

Figure 3. A rigid rotation of the βth block by an amount $\Delta\theta^{(\beta)}$ about an axis parallel to the unit vector $\boldsymbol{\rho}^{(\beta)}$, which is parallel to the local coordinate axis $\xi_2^{(\alpha)}$. The rotation rotates the material lines parallel to the unit vectors $\mathbf{H}_1^{(\beta)}$ and $\mathbf{H}_3^{(\beta)}$ into the orientations parallel to $\mathbf{h}_1^{(\beta)}$ and $\mathbf{h}_3^{(\beta)}$. The rotation is described by the component of the rotation tensor $\tilde{R}_{13}^{(\beta)}$, which is a component of the antisymmetric part of the block-rotation displacement gradient tensor $\frac{\partial\tilde{\upsilon}_k^{(\beta)}}{\partial\xi_l^{(\alpha)}}$. This tensor defines the rotation of the block about its centroid: $\tilde{R}_{13}^{(\beta)} = \frac{1}{2}\left(\frac{\partial\tilde{\upsilon}_1^{(\beta)}}{\partial\xi_3^{(\alpha)}} - \frac{\partial\tilde{\upsilon}_3^{(\beta)}}{\partial\xi_1^{(\alpha)}}\right)$. The block-rotation displacement gradients for material points in the βth block relative to the local coordinates for the αth surface are of equal magnitude but opposite sign. Thus, $\frac{\partial\tilde{\upsilon}_1^{(\beta)}}{\partial\xi_3^{(\alpha)}} = -\frac{\partial\tilde{\upsilon}_3^{(\beta)}}{\partial\xi_1^{(\alpha)}} = \tan\Delta\theta^{(\beta)} \approx \Delta\theta^{(\beta)} = \tilde{R}_{13}^{(\beta)}$, where we have used the approximation for $\tan\Delta\theta^{(\beta)}$ if $\Delta\theta^{(\beta)} \ll 1$.

which shows that $\tilde{R}_{km}^{(\beta)}$ is antisymmetric. From equation (52) we find the block-rotation increment is given by

$$\tilde{\rho}_k^{(\beta)}\Delta\theta^{(\beta)} = \frac{1}{2}\varepsilon_{klm}\tilde{R}_{ml}^{(\beta)} = \frac{1}{2}\varepsilon_{klm}\tilde{\mathfrak{R}}_{ml}^{(\beta)}. \tag{53}$$

For the special case in Figure 2c,

$$\tilde{\rho}_k^{(\beta)} = \begin{bmatrix} 0 & 1 & 0 \end{bmatrix}. \tag{54}$$

Thus, from equation (53) with (54),

$$\begin{aligned}\tilde{\rho}_2^{(\beta)}\Delta\theta^{(\beta)} = \Delta\theta^{(\beta)} &= \frac{1}{2}[\varepsilon_{231}\tilde{R}_{13}^{(\beta)} + \varepsilon_{213}\tilde{R}_{31}^{(\beta)}] \\ &= \frac{1}{2}[\tilde{R}_{13}^{(\beta)} - \tilde{R}_{31}^{(\beta)}],\end{aligned}$$

$$\tilde{\rho}_2^{(\beta)}\Delta\theta^{(\beta)} = \Delta\theta^{(\beta)} = \tilde{R}_{13}^{(\beta)} = -\tilde{R}_{31}^{(\beta)}, \tag{55}$$

where for equation (55) we used equation (54) and the antisymmetric property of $\tilde{R}_{km}^{(\beta)}$ from equation (52). If $\tilde{\upsilon}_k^{(\beta)}$ is the internal block displacement field that describes the local block rotation of the βth block about its centroid (Fig. 3), then for a local block rotation about an axis parallel to $\boldsymbol{\iota}_2^{(\alpha)}$ (equation 54), $\tilde{R}_{13}^{(\beta)}$ has the same sign as the local internal block displacement gradient $\partial\tilde{\upsilon}_1^{(\beta)}/\partial\xi_3$. A positive value for this gradient gives a positive right-handed rotation about the axis $\tilde{\rho}_2^{(\beta)}$ (Fig. 3).

We can now write the amount of slip on the shear plane due to the local block rotation of the two blocks whose interface is the αth shear plane. We assume the blocks are of equal size so that each centroid is at a distance measured normal to the αth surface of $(\Delta\ell^{(\alpha)}/2)$, and we assume that each block and, thus, the αth surface has the same rotation as just defined for the βth block. The partial slip $\Delta\boldsymbol{\zeta}^{(\alpha)}$ on the αth surface due to the rotation of both blocks is, therefore, twice the slip due to the rotation of one block. Thus, for the block into which the unit normal $\boldsymbol{\eta}^{(\alpha)}$ points,

$$\frac{\Delta\boldsymbol{\zeta}^{(\alpha)}}{2} = \left(\frac{\Delta\ell^{(\alpha)}}{2}\Delta\theta^{(\alpha)}\right)\boldsymbol{\eta}^{(\alpha)} \times \boldsymbol{\rho}^{(\alpha)}. \tag{56}$$

In equation (56), $\Delta\theta^{(\alpha)}\boldsymbol{\rho}^{(\alpha)}$ is the local block rotation of the αth surface. This surface rotates with the βth block for which it is a boundary. Therefore, we have substituted the superscript (α) indicating the αth surface for the (β) used previously for the βth block. The term $\frac{\Delta\ell^{(\alpha)}}{2}\Delta\theta^{(\alpha)}$ is the distance a point on the αth surface is translated by the rotation, and $\boldsymbol{\eta}^{(\alpha)} \times \boldsymbol{\rho}^{(\alpha)}$ is the direction parallel to the αth surface, which is normal to the rotation axis. Thus, equation (56) defines the amount of slip parallel to the surface due to the component of the rotation of the surface about the rotation axis of the block. For example, if $\boldsymbol{\rho}^{(\alpha)} = \boldsymbol{\iota}_2^{(\alpha)}$, a positive local block rotation results in a slip that has the opposite shear sense to that of a positive local centroid deformation (Fig. 2b, c). In com-

ponent notation we can write the slip on the αth surface from local block rotation using equation (56), as

$$\Delta\tilde{\zeta}_l^{(\alpha)} = \varepsilon_{lmp}\tilde{\eta}_m^{(\alpha)}\tilde{\rho}_p^{(\alpha)}\Delta\theta^{(\alpha)}\Delta\ell^{(\alpha)}. \tag{57}$$

The slip components contributed by the local centroid deformation, equation (18), and by the local block rotation, equation (57), both depend linearly on the dimension of the block $\Delta\ell^{(\alpha)}$, so the ratio of these two partial slip components and the orientation of the complete slip vector do not depend on the block size.

For the special case illustrated in Figure 2, the fourth part of equation (11) and equation (54) require that the only nonzero values of equation (57) are for

$$\varepsilon_{lmp} = \varepsilon_{132} = -1.$$

Substituting this result into equation (57) shows that for this special case the contribution of the local block rotation to the slip vector on the αth surface is

$$\Delta\tilde{\zeta}_k^{(\alpha)} = \begin{bmatrix} -\Delta\theta^{(\alpha)} & 0 & 0 \end{bmatrix}\Delta\ell^{(\alpha)} \quad \text{if } \tilde{\rho}_k^{(\alpha)} = \begin{bmatrix} 0 & 1 & 0 \end{bmatrix}. \tag{58}$$

We can transform equation (57) into common coordinates by using the transformations in equation (9) and then simplify using equation (8) to find

$$\Delta\zeta_k^{(\alpha)} = \varepsilon_{klm}\eta_l^{(\alpha)}\rho_m^{(\alpha)}\Delta\theta^{(\alpha)}\Delta\ell^{(\alpha)}. \tag{59}$$

We can express this result in terms of the local instantaneous block-rotation tensor by transforming equation (52) into common coordinates using the transformations defined in equation (9) and recognizing that the alternating tensor (equation 50) is invariant under orthogonal transformation. We find

$$R_{mk}^{(\alpha)} = \varepsilon_{kmn}\rho_n^{(\alpha)}\Delta\theta^{(\alpha)} = -R_{km}^{(\alpha)}. \tag{60}$$

Introducing equation (60) into (59) gives

$$\Delta\zeta_k^{(\alpha)} = R_{mk}^{(\alpha)}\eta_m^{(\alpha)}\Delta\ell^{(\alpha)} = -R_{km}^{(\alpha)}\eta_m^{(\alpha)}\Delta\ell^{(\alpha)}. \tag{61}$$

Contribution of the Local Block Rotation to the Local Micropolar Moment Tensor. The contribution of the local block rotation to the local micropolar moment tensor is ${}_{(r)}\tilde{m}_{kl}^{(\alpha)}$, where the left subscript (r) identifies the rotational component; it is given by an equation comparable to equation (27):

$${}_{(r)}\tilde{m}_{kl}^{(\alpha)} = \Delta\tilde{\zeta}_k^{(\alpha)}\tilde{\eta}_l^{(\alpha)}S^{(\alpha)}. \tag{62}$$

Using equations (57) and (29) in (62) and then using equation (52), we find

$${}_{(r)}\tilde{m}_{kl}^{(\alpha)} = \varepsilon_{kmp}\tilde{\eta}_m^{(\alpha)}\tilde{\rho}_p^{(\alpha)}\tilde{\eta}_l^{(\alpha)}\Delta\theta^{(\alpha)}V^{(\alpha)} = \tilde{R}_{mk}^{(\alpha)}\tilde{\eta}_m^{(\alpha)}\tilde{\eta}_l^{(\alpha)}V^{(\alpha)}. \tag{63}$$

For the special case in Figure 2, for which we assume equation (54), we see from the fourth part of equation (11) that the only nonzero components of this part of the local micropolar moment tensor are those for which the subscripts take the values $p = 2$ and $l = m = 3$, which because of the alternating tensor (equation 50), requires $k = 1$. Thus, from equation (63) we find for the special case in Figure 2

$$\begin{aligned} {}_{(r)}\tilde{m}_{kl}^{(\alpha)} &= \begin{bmatrix} 0 & 0 & -\tilde{\rho}_2^{(\alpha)}\Delta\theta^{(\alpha)} \\ 0 & 0 & 0 \\ 0 & 0 & 0 \end{bmatrix} V^{(\alpha)} \\ &= \begin{bmatrix} 0 & 0 & \tilde{R}_{31}^{(\alpha)} \\ 0 & 0 & 0 \\ 0 & 0 & 0 \end{bmatrix} V^{(\alpha)}, \end{aligned} \tag{64}$$

which shows that the component of the local micropolar moment tensor contributed by the local block rotation is defined just by the local instantaneous block-rotation tensor.

We now wish to transform the components of the local micropolar moment tensor from the local coordinates $\xi_k^{(\alpha)}$, which are tied to the orientation of the slip plane, to the common geographic coordinate system x_k so that we can add the components from all the slip events in a volume. To this end we use the orthogonal transformation defined in equation (8) and the form for the transformation of a second rank tensor in equation (9) with equation (63) to write the local block-rotational component of the local micropolar moment tensor as

$${}_{(r)}m_{kl}^{(\alpha)} = \varepsilon_{kmn}\eta_m^{(\alpha)}\rho_n^{(\alpha)}\eta_l^{(\alpha)}\Delta\theta^{(\alpha)}V^{(\alpha)} = R_{mk}^{(\alpha)}\eta_m^{(\alpha)}\eta_l^{(\alpha)}V^{(\alpha)}. \tag{65}$$

Contribution of the Microrotation to the Micropolar Moment-Density Tensor. We now want to sum the local block-rotational components of the local micropolar moment tensors for all the N slip events in the volume $\mathcal{V}$ to obtain the local block-rotational contribution to the micropolar moment-density tensor for the volume

$${}_{(r)}\mathcal{M}_{ij} \equiv \frac{1}{\mathcal{V}}\sum_{\alpha=1}^{N} {}_{(r)}m_{ij}^{(\alpha)}. \tag{66}$$

Using equation (65) in (66) gives

$$\begin{aligned} {}_{(r)}\mathcal{M}_{ij} &\equiv \frac{1}{\mathcal{V}}\sum_{\alpha=1}^{N} \varepsilon_{imn}\eta_m^{(\alpha)}\rho_n^{(\alpha)}\eta_j^{(\alpha)}\Delta\theta^{(\alpha)}V^{(\alpha)} \\ &= \frac{1}{\mathcal{V}}\sum_{\alpha=1}^{N} R_{mi}^{(\alpha)}\eta_m^{(\alpha)}\eta_j^{(\alpha)}V^{(\alpha)}. \end{aligned} \tag{67}$$

By analogy with the definitions for the macrodisplacement gradient equation (38), we define the instantaneous microrotation by

$$\mathcal{R}_{ij} \equiv \frac{1}{\mathcal{V}} \sum_{\alpha=1}^{N} R_{im}^{(\alpha)} \eta_m^{(\alpha)} \eta_j^{(\alpha)} V^{(\alpha)}$$
$$= -\frac{1}{\mathcal{V}} \sum_{\alpha=1}^{N} \varepsilon_{imn} \eta_m^{(\alpha)} \rho_n^{(\alpha)} \eta_j^{(\alpha)} \Delta\theta^{(\alpha)} V^{(\alpha)}, \qquad (68)$$

where we used equation (60) to find the second relation. Equations (67) and (68) with equation (60) then give

$$_{(r)}\mathcal{M}_{ij} = -\mathcal{R}_{ij}. \qquad (69)$$

It is not immediately obvious from equation (68) that $\mathcal{R}_{ij}$ is antisymmetric even though $R_{im}^{(\alpha)}$ is (equation 60). In equation (68) the terms for each shear plane α are summed over all N shear planes in the volume $\mathcal{V}$ on which slip events have occurred. For sufficiently large N, we assume the sum will include events on planes that have a similar distribution of orientations to that for the surfaces surrounding an average block. Thus, we can consider that the summation over a sufficiently large number of events N is statistically equivalent to the summation over all the bounding surfaces of a large number of rigid blocks, and under those circumstances, $\mathcal{R}_{ij}$ approaches being an antisymmetric tensor (see Appendix B):

$$\lim_{N\gg 1}(\mathcal{R}_{ij}) = \frac{1}{\mathcal{V}} \lim_{N\gg 1}\left[\sum_{\alpha=1}^{N} R_{im}^{(\alpha)} \eta_m^{(\alpha)} \eta_j^{(\alpha)} V^{(\alpha)}\right] \to \mathcal{R}_{[ij]}. \qquad (70)$$

Thus, in the limit of a large number of events we have

$$\mathcal{R}_{ij} \approx -\mathcal{R}_{ji}, \qquad _{(r)}\mathcal{M}_{ij} \approx -_{(r)}\mathcal{M}_{ji}. \qquad (71)$$

The Complete Micropolar Moment Tensor

The Complete Local Slip Vector. The complete slip vector $\Delta\mathbf{v}^{(\alpha)}$ on the αth surface (Fig. 2d) is the sum of the slip components contributed by the local centroid deformation (Fig. 2b) and the local block rotation (Fig. 2c):

$$\Delta\mathbf{v}^{(\alpha)} = \Delta\mathbf{z}^{(\alpha)} + \Delta\boldsymbol{\zeta}^{(\alpha)}. \qquad (72)$$

In the local coordinates, the components of the complete slip vector are given from equations (18) and (57) by

$$\Delta\tilde{v}_l^{(\alpha)} = \left\{\frac{\partial\tilde{u}_k^{(\alpha)}}{\partial\xi_m^{(\alpha)}} - \left[\frac{\partial\tilde{u}_i^{(\alpha)}}{\partial\xi_j^{(\alpha)}}\tilde{\eta}_i^{(\alpha)}\tilde{\eta}_j^{(\alpha)}\right]\delta_{km}\right\}\tilde{\eta}_m^{(\alpha)}\Delta\ell^{(\alpha)}$$
$$+ \varepsilon_{imp}\tilde{\eta}_m^{(\alpha)}\tilde{\rho}_p^{(\alpha)}\Delta\theta^{(\alpha)}\Delta\ell^{(\alpha)}. \qquad (73)$$

For the special case illustrated in Figure 2, these components are, from equations (22) and (58),

$$\Delta\tilde{v}_l^{(\alpha)} = \begin{bmatrix} \left(\frac{\partial\tilde{u}_1^{(\alpha)}}{\partial\xi_3^{(\alpha)}} - \Delta\theta^{(\alpha)}\right) & 0 & 0 \end{bmatrix}\Delta\ell^{(\alpha)}, \qquad (74)$$

which shows that the complete slip is the contribution from the local centroid deformation reduced by the contribution from the local block rotation if both contributions are positive.

In common coordinates the expression for the complete slip vector, as defined by equation (72), is found by adding together equations (23) and either (59) or (61):

$$\Delta v_k^{(\alpha)} = \{u_{k,m}^{(\alpha)} - [u_{i,j}^{(\alpha)}\eta_i^{(\alpha)}\eta_j^{(\alpha)}]\delta_{km}\}\eta_m^{(\alpha)}\Delta\ell^{(\alpha)}$$
$$+ \varepsilon_{kmj}\eta_m^{(\alpha)}\rho_j^{(\alpha)}\Delta\theta^{(\alpha)}\Delta\ell^{(\alpha)}, \qquad (75)$$

$$\Delta v_k^{(\alpha)} = \Delta\ell^{(\alpha)}\{[u_{i,m}^{(\alpha)}\eta_m^{(\alpha)}(\delta_{ik} - \eta_i^{(\alpha)}\eta_k^{(\alpha)})] - R_{km}^{(\alpha)}\eta_m^{(\alpha)}\}. \qquad (76)$$

In deriving equation (76), we used the antisymmetric property of $R_{mk}^{(\alpha)}$ (equation 60) to keep subscripts in a consistent order.

We can express the components of the complete slip vector as a scalar magnitude $\Delta v^{(\alpha)}$ times the components of a unit vector $\nu_k^{(\alpha)}$,

$$\Delta v_k^{(\alpha)} \equiv \Delta v^{(\alpha)}\nu_k^{(\alpha)}, \qquad \Delta v^{(\alpha)} \equiv [\Delta v_k^{(\alpha)}\Delta v_k^{(\alpha)}]^{1/2},$$
$$\nu_k^{(\alpha)} \equiv \frac{\Delta v_k^{(\alpha)}}{\Delta v^{(\alpha)}}, \qquad \nu_k^{(\alpha)}\nu_k^{(\alpha)} = 1, \qquad (77)$$

whereby we can solve equation (76) for the components of the unit vector that parallels the slip direction:

$$\nu_k^{(\alpha)} = \frac{\Delta\ell^{(\alpha)}}{\Delta v^{(\alpha)}}\{[u_{i,m}^{(\alpha)}\eta_m^{(\alpha)}(\delta_{ik} - \eta_i^{(\alpha)}\eta_k^{(\alpha)})] - R_{km}^{(\alpha)}\eta_m^{(\alpha)}\}. \qquad (78)$$

Then, separating the local centroid displacement gradients and local block rotations in equation (78) into symmetric and antisymmetric parts using the notation in equation (3) gives

$$\nu_k^{(\alpha)} = \frac{\Delta\ell^{(\alpha)}}{\Delta v^{(\alpha)}}\{[u_{(i,m)}^{(\alpha)}(\delta_{ik} - \eta_i^{(\alpha)}\eta_k^{(\alpha)})] + [u_{[k,m]}^{(\alpha)} - R_{km}^{(\alpha)}]\}\eta_m^{(\alpha)}, \qquad (79)$$

where we have used the fact that the scalar product of an antisymmetric tensor $u_{[i,m]}^{(\alpha)}$ with a symmetric tensor $\eta_i^{(\alpha)}\eta_m^{(\alpha)}$ must be zero.

For future convenience in comparing this result with the result from the continuum micropolar analysis (Twiss *et al.*, 1991, 1993), we note that, by using the symmetric property of $u_{(i,m)}^{(\alpha)}$ and the antisymmetric property of $u_{[k,m]}^{(\alpha)}$ and $R_{km}^{(\alpha)}$ (equation 60), we can also write equation (79) in the form

$$\nu_k^{(\alpha)} = \frac{\Delta\ell^{(\alpha)}}{\Delta v^{(\alpha)}}\{[u_{(m,i)}^{(\alpha)}(\delta_{ik} - \eta_i^{(\alpha)}\eta_k^{(\alpha)})] + [R_{mk}^{(\alpha)} - u_{[m,k]}^{(\alpha)}]\}\eta_m^{(\alpha)}. \qquad (80)$$

The Complete Local Micropolar Moment Tensor. The complete local micropolar moment tensor is obtained for the discrete-block model by summing the contributions from

the local centroid deformation and the local block rotation for a single slip event. In the local coordinates $\xi_k^{(\alpha)}$ for the αth event, we have

$$\begin{aligned}\tilde{m}_{kl}^{(\alpha)} &= \Delta\tilde{v}_k^{(\alpha)}\tilde{\eta}_l^{(\alpha)}S^{(\alpha)},\\ \tilde{m}_{kl}^{(\alpha)} &= [\Delta\tilde{z}_k^{(\alpha)} + \Delta\tilde{\zeta}_k^{(\alpha)}]\tilde{\eta}_l^{(\alpha)}S^{(\alpha)},\\ \tilde{m}_{kl}^{(\alpha)} &= {}_{(d)}\tilde{m}_{kl}^{(\alpha)} + {}_{(r)}\tilde{m}_{kl}^{(\alpha)}.\end{aligned} \tag{81}$$

Each of these three equations leads to the same result: Using the first part of equation (81) with (73) and (29), or using the second part of equation (81) with equations (18) and (57), or using the third part of equation (81) with equations (28) and (63)—each gives

$$\begin{aligned}\tilde{m}_{kl}^{(\alpha)} = \Bigg\{&\frac{\partial\tilde{u}_k^{(\alpha)}}{\partial\xi_m^{(\alpha)}}\tilde{\eta}_m^{(\alpha)}\tilde{\eta}_l^{(\alpha)} - \left[\frac{\partial\tilde{u}_i^{(\alpha)}}{\partial\xi_j^{(\alpha)}}\tilde{\eta}_i^{(\alpha)}\tilde{\eta}_j^{(\alpha)}\right]\tilde{\eta}_k^{(\alpha)}\tilde{\eta}_l^{(\alpha)}\\ &+ \left[\varepsilon_{kmp}\tilde{\eta}_m^{(\alpha)}\tilde{\rho}_p^{(\alpha)}\right]\tilde{\eta}_l^{(\alpha)}\Delta\theta^{(\alpha)}\Bigg\}V^{(\alpha)}.\end{aligned} \tag{82}$$

Then using equation (63) gives

$$\begin{aligned}\tilde{m}_{kl}^{(\alpha)} = \Bigg\{&\frac{\partial\tilde{u}_k^{(\alpha)}}{\partial\xi_m^{(\alpha)}}\tilde{\eta}_m^{(\alpha)}\tilde{\eta}_l^{(\alpha)} - \left[\frac{\partial\tilde{u}_i^{(\alpha)}}{\partial\xi_j^{(\alpha)}}\tilde{\eta}_i^{(\alpha)}\tilde{\eta}_j^{(\alpha)}\right]\tilde{\eta}_k^{(\alpha)}\tilde{\eta}_l^{(\alpha)}\\ &- \tilde{R}_{km}^{(\alpha)}\tilde{\eta}_m^{(\alpha)}\tilde{\eta}_l^{(\alpha)}\Bigg\}V^{(\alpha)}.\end{aligned} \tag{83}$$

For the special case illustrated in Figure 2, we use the fact that $\tilde{u}_2^{(\alpha)} = 0$ along with the fourth part of equation (11) and equation (54) in equations (82) and (83) to find the components of the complete local micropolar moment tensor

$$\begin{aligned}\tilde{m}_{kl}^{(\alpha)} &= \begin{bmatrix} 0 & 0 & (\frac{\partial\tilde{u}_1^{(\alpha)}}{\partial\xi_3^{(\alpha)}} - \Delta\theta^{(\alpha)}) \\ 0 & 0 & 0 \\ 0 & 0 & 0 \end{bmatrix} V^{(\alpha)}\\ &= \begin{bmatrix} 0 & 0 & (\frac{\partial\tilde{u}_1^{(\alpha)}}{\partial\xi_3^{(\alpha)}} - \tilde{R}_{13}^{(\alpha)}) \\ 0 & 0 & 0 \\ 0 & 0 & 0 \end{bmatrix} V^{(\alpha)}.\end{aligned} \tag{84}$$

The symmetric and antisymmetric parts of this tensor in the local coordinates are

$$\tilde{m}_{(kl)}^{(\alpha)} = \begin{bmatrix} 0 & 0 & \frac{1}{2}(\frac{\partial\tilde{u}_1^{(\alpha)}}{\partial\xi_3^{(\alpha)}} - \tilde{R}_{13}^{(\alpha)}) \\ 0 & 0 & 0 \\ \frac{1}{2}(\frac{\partial\tilde{u}_1^{(\alpha)}}{\partial\xi_3^{(\alpha)}} - \tilde{R}_{13}^{(\alpha)}) & 0 & 0 \end{bmatrix} V^{(\alpha)}, \tag{85}$$

$$\tilde{m}_{[kl]}^{(\alpha)} = \begin{bmatrix} 0 & 0 & \frac{1}{2}(\frac{\partial\tilde{u}_1^{(\alpha)}}{\partial\xi_3^{(\alpha)}} - \tilde{R}_{13}^{(\alpha)}) \\ 0 & 0 & 0 \\ -\frac{1}{2}(\frac{\partial\tilde{u}_1^{(\alpha)}}{\partial\xi_3^{(\alpha)}} - \tilde{R}_{13}^{(\alpha)}) & 0 & 0 \end{bmatrix} V^{(\alpha)}. \tag{86}$$

In the common geographic coordinates, the first and third parts of equation (81) have the forms

$$m_{kl}^{(\alpha)} = \Delta v_k^{(\alpha)}\eta_l^{(\alpha)}S^{(\alpha)}, \tag{87}$$

$$m_{kl}^{(\alpha)} = {}_{(d)}m_{kl}^{(\alpha)} + {}_{(r)}m_{kl}^{(\alpha)}. \tag{88}$$

From equations (75) and (76) with (87) and (29) or from equations (33) and (65) with (88), we find

$$\begin{aligned}m_{kl}^{(\alpha)} = &\{u_{k,m}^{(\alpha)}\eta_m^{(\alpha)}\eta_l^{(\alpha)} - [u_{i,j}^{(\alpha)}\eta_i^{(\alpha)}\eta_j^{(\alpha)}]\eta_k^{(\alpha)}\eta_l^{(\alpha)}\}V^{(\alpha)}\\ &+ [\varepsilon_{kmn}\eta_m^{(\alpha)}\rho_n^{(\alpha)}]\eta_l^{(\alpha)}\Delta\theta^{(\alpha)}V^{(\alpha)},\end{aligned} \tag{89}$$

$$\begin{aligned}m_{kl}^{(\alpha)} = &\{u_{k,m}^{(\alpha)}\eta_m^{(\alpha)}\eta_l^{(\alpha)} - [u_{i,j}^{(\alpha)}\eta_i^{(\alpha)}\eta_j^{(\alpha)}]\eta_k^{(\alpha)}\eta_l^{(\alpha)}\}V^{(\alpha)}\\ &- R_{km}^{(\alpha)}\eta_m^{(\alpha)}\eta_l^{(\alpha)}V^{(\alpha)}.\end{aligned} \tag{90}$$

Separating the complete local micropolar moment tensor into symmetric and antisymmetric parts with respect to the indices k and l and using the notation defined in equation (3) gives

$$\begin{aligned}m_{kl}^{(\alpha)} = &\{u_{(k,m}^{(\alpha)}\eta_m^{(\alpha)}\eta_{l)}^{(\alpha)} - [u_{i,j}^{(\alpha)}\eta_i^{(\alpha)}\eta_j^{(\alpha)}]\eta_k^{(\alpha)}\eta_l^{(\alpha)}\\ &- R_{(km}^{(\alpha)}\eta_m^{(\alpha)}\eta_{l)}^{(\alpha)}\}V^{(\alpha)} + \{[u_{[k,m}^{(\alpha)} - R_{[km}^{(\alpha)}]\eta_m^{(\alpha)}\eta_{l]}^{(\alpha)}\}V^{(\alpha)},\end{aligned} \tag{91}$$

where the term in the first set of braces $\{\ldots\}$ is the symmetric part and the term in the second set of braces $\{\ldots\}$ is the antisymmetric part.

Equation (91) defines the complete local micropolar moment tensor for a single seismic event, which includes the effects of both a local centroid deformation and a local block rotation. It is clear from the form of this equation that this tensor is asymmetric. Furthermore, equation (91) and its form for the special case of Figure 2, which is given in the local coordinates by equations (85) and (86), make it clear that the symmetric part of the local micropolar moment tensor for an individual seismic event is affected by the antisymmetric local block rotation $R_{lm}^{(\alpha)}$. In essence, both the local centroid deformation and the local block rotation contribute to the slip on the fault plane, and this slip is the essential term in the definition of the classical symmetric moment tensor for a single slip event. Because the orientation of the seismic P and T axes for the standard focal mechanism solution is based on an assumption of a symmetric moment tensor for each event, equation (91) shows how the orienta-

tions of those axes include information about the local block rotation.

The Complete Micropolar Moment-Density Tensor. The complete micropolar moment-density tensor $\mathcal{M}_{kl}$ is simply the volume-averaged sum of the local micropolar moment tensors, which are contributed by the local centroid deformations and the local block rotations within that volume. This sum can be expressed in a number of ways, all of which lead to the same result:

$$\mathcal{M}_{kl} \equiv \frac{1}{\mathcal{V}} \sum_{\alpha=1}^{N} m_{kl}^{(\alpha)}. \tag{92}$$

From equations (92) and (87),

$$\mathcal{M}_{kl} = \frac{1}{\mathcal{V}} \sum_{\alpha=1}^{N} \Delta v_k^{(\alpha)} \eta_l^{(\alpha)} S^{(\alpha)}. \tag{93}$$

From equations (92) and (88),

$$\mathcal{M}_{kl} = \frac{1}{\mathcal{V}} \sum_{\alpha=1}^{N} [{}_{(d)}m_{kl}^{(\alpha)} + {}_{(r)}m_{kl}^{(\alpha)}]. \tag{94}$$

From equations (93) and (72),

$$\mathcal{M}_{kl} = \frac{1}{\mathcal{V}} \sum_{\alpha=1}^{N} [\Delta z_k^{(\alpha)} + \Delta \zeta_k^{(\alpha)}] \eta_l^{(\alpha)} S^{(\alpha)}. \tag{95}$$

From equations (94), (36), and (66),

$$\mathcal{M}_{kl} = {}_{(d)}\mathcal{M}_{kl} + {}_{(r)}\mathcal{M}_{kl}. \tag{96}$$

Using equation (92) with either (89) or (90); or using equation (93) with either (75) or (76) and (29); or using equation (94) with (33) and (65); or using equation (95) with (23) and either (59) or (61); or using equation (96) with (37) and (67), we find the same result for the complete micropolar moment-density tensor:

$$\mathcal{M}_{kl} = \frac{1}{\mathcal{V}} \sum_{\alpha=1}^{N} \{[u_{k,m}^{(\alpha)} \eta_m^{(\alpha)} \eta_l^{(\alpha)} - (u_{i,j}^{(\alpha)} \eta_i^{(\alpha)} \eta_j^{(\alpha)}) \eta_k^{(\alpha)} \eta_l^{(\alpha)}] + \varepsilon_{kmn} \eta_m^{(\alpha)} \rho_n^{(\alpha)} \eta_l^{(\alpha)} \Delta\theta^{(\alpha)}\} V^{(\alpha)}, \tag{97}$$

$$\mathcal{M}_{kl} = \frac{1}{\mathcal{V}} \sum_{\alpha=1}^{N} \{[u_{k,m}^{(\alpha)} \eta_m^{(\alpha)} \eta_l^{(\alpha)} - (u_{i,j}^{(\alpha)} \eta_i^{(\alpha)} \eta_j^{(\alpha)}) \eta_k^{(\alpha)} \eta_l^{(\alpha)}] - R_{km}^{(\alpha)} \eta_m^{(\alpha)} \eta_l^{(\alpha)}\} V^{(\alpha)}. \tag{98}$$

Introducing equations (38), (39), and (68) into equation (98) gives

$$\mathcal{M}_{kl} = (u_{k,l} - \Phi_{kl}) - \mathcal{R}_{kl}. \tag{99}$$

This result is identical to the result we get from equation (96) with equations (43) and (69).

Then, using equation (45) in equation (99), we find

$$\mathcal{M}_{kl} = (e_{kl} - \Phi_{kl}) + [r_{kl} - \mathcal{R}_{kl}], \tag{100}$$

where the parentheses (…) and brackets […] contain the symmetric and the antisymmetric parts of the tensor, respectively. This equation shows that, in averaging the complete local micropolar moment tensor over the volume $\mathcal{V}$ (equation 92 with 91), the dependence of the symmetric part of moment-density tensor on the local block rotation drops out, because the average of the local block rotations is antisymmetric (equations 70 and B5).

For later convenience in comparing these results with those of the continuum micropolar model, we define the transpose of the micropolar moment-density tensor:

$$\mathcal{M}_{kl}^{\mathrm{T}} \equiv \mathcal{M}_{lk}. \tag{101}$$

Using equation (100) in (101), and then using the symmetry of the macrostrain tensor (equation 44) and the antisymmetry of both the macrorotation (equation 44) and microrotation tensors (equations 71 and B5), we find

$$\mathcal{M}_{kl}^{\mathrm{T}} = (e_{kl} - \Phi_{kl}) + [\mathcal{R}_{kl} - r_{kl}]. \tag{102}$$

Thus, the symmetric part of the micropolar moment-density tensor is the isochoric macrostrain, and the antisymmetric part is the relative rotation. Because the relative rotation is the difference between two rotations (specifically, the macrorotation and the microrotation), it is an objective quantity, which means that it is independent of the translation or rotation of the coordinate system in which it is described.

Comparison of the Discrete-Block and Continuum Models of Deformation

In the subsequent discussion, we compare the results from the continuum micropolar and the discrete-block models of the deformation in materials with substructure. We use an overbar on the symbols for the continuum micropolar variables to distinguish them from similar symbols for comparable variables used in the discrete-block analysis.

Comparison of the Slip Vectors. In the continuum micropolar analysis, the unit vector $\bar{\boldsymbol{\nu}}^{(\alpha)}$ is parallel to the slip velocity vector on the αth shear plane, for which the unit normal is $\boldsymbol{\eta}^{(\alpha)}$. It is calculated by (Twiss *et al.*, 1993, from their equations 7 and 9)

$$\bar{\nu}_m^{(\alpha)} = \frac{1}{\bar{L}} \{\bar{d}_{kl} \eta_k^{(\alpha)} [\delta_{lm} - \eta_l^{(\alpha)} \eta_m^{(\alpha)}] + (\bar{\omega}_{km} - \bar{w}_{km}) \eta_k^{(\alpha)}\}. \tag{103}$$

The quantity in braces {…} defines the components of the slip velocity vector per unit distance normal to the shear

plane, and $\bar{L}$ is the magnitude of that vector. $\bar{d}_{kl}$ and $\bar{w}_{km}$ are, respectively, the macrodeformation rate tensor and the macrospin tensor, which are the symmetric and antisymmetric parts of the macrovelocity gradient tensor, and $\bar{\omega}_{km}$ is the microspin tensor. These tensor rates, when multiplied by an infinitesimal increment of time dt, yield the macrostrain, macrorotation, and the microrotation, respectively:

$$\bar{e}_{kl} = \bar{e}_{lk} = \bar{d}_{kl}\,dt, \qquad \bar{r}_{kl} = -\bar{r}_{lk} = \bar{w}_{kl}\,dt, \qquad \bar{\mathcal{R}}_{kl} = -\bar{\mathcal{R}}_{lk} = \bar{\omega}_{kl}\,dt, \tag{104}$$

where the macrodisplacement gradient is given by

$$\bar{u}_{k,l} \equiv \bar{e}_{kl} + \bar{r}_{kl}. \tag{105}$$

Thus, multiplying the right-hand side of equation (103) by dt/dt and using equation (104) gives

$$\bar{\nu}_m^{(\alpha)} = \frac{1}{\bar{L}dt}\{\bar{e}_{kl}\eta_k^{(\alpha)}[\delta_{lm} - \eta_l^{(\alpha)}\eta_m^{(\alpha)}] + (\bar{\mathcal{R}}_{km} - \bar{r}_{km})\eta_k^{(\alpha)}\}. \tag{106}$$

We see that equation (106) for the continuum model has exactly the same form as equation (80) for the discrete-block model if

$$\frac{\Delta v^{(\alpha)}}{\Delta \ell^{(\alpha)}} = \bar{L}dt. \tag{107}$$

Equation (107) equates two dimensionless expressions defining the magnitude of the local centroid displacement per unit distance normal to the slip surface. The left-hand side is for the discrete-block model; the right-hand side is from the continuum micropolar model. The difference between equations (80) and (106) and between the two terms in equation (107) is that, for the discrete-block model, the symmetric and antisymmetric parts of the centroid displacement gradient and the block rotation are all the local quantities associated with the particular slip event. For the continuum model, however, the macrostrain, macrorotation, and microrotation are in effect the volume-averaged quantities, which are defined by equation (38) with (44) and (45) and by equation (68). Thus, on average we expect

$$\nu_m^{(\alpha)} \approx \bar{\nu}_m^{(\alpha)}, \tag{108}$$

and the present discrete-block model gives essentially the same result as the earlier continuum model. The present approach, however, provides an explicit physical model by which the micropolar kinematic variables associated with slip on a specific shear plane can be associated with the micropolar moment tensor, as detailed in the following analysis.

Comparison of the Continuum and Discrete-Block Models for the Local Micropolar Moment Tensor. The local micropolar moment tensor for an individual event is defined in the continuum micropolar model by

$$\bar{m}_{kl}^{(\alpha)} \equiv \bar{M}_0^{(\alpha)}\bar{\nu}_k^{(\alpha)}\eta_l^{(\alpha)} = \bar{\lambda}^{(\alpha)}\bar{\nu}_k^{(\alpha)}\eta_l^{(\alpha)}S^{(\alpha)}, \qquad \bar{M}_0^{(\alpha)} \equiv \bar{\lambda}^{(\alpha)}S^{(\alpha)}. \tag{109}$$

$\bar{M}_0^{(\alpha)}$ is the local scalar geometric moment, $\bar{\nu}_k^{(\alpha)}$ and $\eta_l^{(\alpha)}$ are unit vectors parallel, respectively, to the slip direction and the normal to the shear plane, and $\bar{\lambda}^{(\alpha)}$ is the magnitude of the slip vector averaged over the area $S^{(\alpha)}$ of the αth shear plane. The classical seismic moment tensor for a single seismic event is just the symmetric part of the micropolar moment tensor multiplied by the shear modulus μ.

For the continuum model, we use equation (106) in (109) to find

$$\bar{m}_{kl}^{(\alpha)} = \{\bar{e}_{mj}\eta_m^{(\alpha)}[\delta_{jk} - \eta_j^{(\alpha)}\eta_k^{(\alpha)}]\eta_l^{(\alpha)} + (\bar{\mathcal{R}}_{mk} - \bar{r}_{mk})\eta_m^{(\alpha)}\eta_l^{(\alpha)}\}\frac{\bar{\lambda}^{(\alpha)}}{\bar{L}dt}S^{(\alpha)}. \tag{110}$$

We can use the symmetric properties of the macrostrain tensor and the antisymmetric properties of both the macrorotation and microrotation tensors (equation 104), and then adjust the letters that are used as dummy indices, to rewrite equation (110) as

$$\bar{m}_{kl}^{(\alpha)} = \{[\bar{e}_{km}\eta_m^{(\alpha)}\eta_l^{(\alpha)} - (\bar{e}_{ij}\eta_i^{(\alpha)}\eta_j^{(\alpha)})\eta_k^{(\alpha)}\eta_l^{(\alpha)}] + (\bar{r}_{km} - \bar{\mathcal{R}}_{km})\eta_m^{(\alpha)}\eta_l^{(\alpha)}\}\frac{\bar{\lambda}^{(\alpha)}}{\bar{L}dt}S^{(\alpha)}. \tag{111}$$

The local micropolar moment tensor for an individual event on the αth shear plane is given for the discrete-block model by equation (90), which can be rewritten for comparison with equation (111) as

$$m_{kl}^{(\alpha)} = \{[u_{(km)}^{(\alpha)}\eta_m^{(\alpha)}\eta_l^{(\alpha)} - (u_{(ij)}^{(\alpha)}\eta_i^{(\alpha)}\eta_j^{(\alpha)})\eta_k^{(\alpha)}\eta_l^{(\alpha)}] + [u_{[km]}^{(\alpha)} - R_{km}^{(\alpha)}]\eta_m^{(\alpha)}\eta_l^{(\alpha)}\}V^{(\alpha)}. \tag{112}$$

Using equation (29) in equation (112), we see that equations (111) and (112) have the same form if

$$\frac{\bar{\lambda}^{(\alpha)}}{\bar{L}dt} = \Delta\ell^{(\alpha)} \quad \text{or} \quad \frac{\bar{\lambda}^{(\alpha)}}{\Delta\ell^{(\alpha)}} = \bar{L}dt. \tag{113}$$

Equation (113) is consistent with the definition in equation (107) with $\Delta v^{(\alpha)} = \bar{\lambda}^{(\alpha)}$.

Equations (111) and (112) differ in that the strains and rotations in equation (111) are the average quantities for the continuum, whereas in equation (112) they are the local values for the slip on the specific αth shear plane. To the extent that the local strains and rotations differ from the average, the equations are not quite the same, but this difference between the two models disappears when we average the individual local events in the discrete-block model over all the events in a volume to compare the micropolar moment-

density tensors for the continuum micropolar model and the discrete-block model, as we show in the next subsection.

Comparison of the Continuum and Discrete-Block Models for the Micropolar Moment-Density Tensor. The micropolar moment-density tensor for the continuum model is defined, analogous to equation (92), by

$$\bar{\mathcal{M}}_{kl} \equiv \frac{1}{\mathcal{V}} \sum_{\alpha=1}^{N} \bar{m}_{kl}^{(\alpha)}. \tag{114}$$

Introducing equation (111), using equations (113) and (29), and rearranging the terms gives

$$\bar{\mathcal{M}}_{kl} \equiv \frac{1}{\mathcal{V}} \sum_{\alpha=1}^{N} \{[\bar{e}_{km}\eta_m^{(\alpha)}\eta_l^{(\alpha)} - (\bar{e}_{ij}\eta_i^{(\alpha)}\eta_j^{(\alpha)})\eta_k^{(\alpha)}\eta_l^{(\alpha)}] + (\bar{r}_{km}\eta_m^{(\alpha)}\eta_l^{(\alpha)} - \bar{\mathcal{R}}_{km}\eta_m^{(\alpha)}\eta_l^{(\alpha)})\} V^{(\alpha)}. \tag{115}$$

We assume that the summation over a sufficiently large number of events N is statistically equivalent to the summation over all the bounding surfaces of a large number of rigid blocks. We can then use equation (A21) to show that the averages of the continuum macrostrain, macrorotation, and microrotation terms in equation (115) are simply the continuum macrostrain, macrorotation, and microrotation themselves:

$$\frac{1}{\mathcal{V}} \sum_{\alpha=1}^{N} \bar{u}_{k,m}\eta_m^{(\alpha)}\eta_l^{(\alpha)} V^{(\alpha)} = \bar{u}_{k,m} \left\{ \frac{1}{\mathcal{V}} \sum_{\alpha=1}^{N} \eta_m^{(\alpha)}\eta_l^{(\alpha)} V^{(\alpha)} \right\} = \bar{u}_{k,m}\delta_{ml} = \bar{u}_{k,l}, \tag{116}$$

$$\frac{1}{\mathcal{V}} \sum_{\alpha=1}^{N} \bar{e}_{km}\eta_m^{(\alpha)}\eta_l^{(\alpha)} V^{(\alpha)} = \bar{e}_{km} \left\{ \frac{1}{\mathcal{V}} \sum_{\alpha=1}^{N} \eta_m^{(\alpha)}\eta_l^{(\alpha)} V^{(\alpha)} \right\} = \bar{e}_{km}\delta_{ml} = \bar{e}_{kl}, \tag{117}$$

$$\frac{1}{\mathcal{V}} \sum_{\alpha=1}^{N} (\bar{u}_{i,j}\eta_i^{(\alpha)}\eta_j^{(\alpha)})\eta_k^{(\alpha)}\eta_l^{(\alpha)} V^{(\alpha)} = \bar{u}_{i,j} \left\{ \frac{1}{\mathcal{V}} \sum_{\alpha=1}^{N} (\eta_i^{(\alpha)}\eta_j^{(\alpha)})\eta_k^{(\alpha)}\eta_l^{(\alpha)} V^{(\alpha)} \right\} \equiv \bar{\Phi}_{kl}, \tag{118}$$

$$\frac{1}{\mathcal{V}} \sum_{\alpha=1}^{N} \bar{r}_{km}\eta_m^{(\alpha)}\eta_l^{(\alpha)} V^{(\alpha)} = \bar{r}_{km} \left\{ \frac{1}{\mathcal{V}} \sum_{\alpha=1}^{N} \eta_m^{(\alpha)}\eta_l^{(\alpha)} V^{(\alpha)} \right\} = \bar{r}_{km}\delta_{ml} = \bar{r}_{kl}, \tag{119}$$

$$\frac{1}{\mathcal{V}} \sum_{\alpha=1}^{N} \bar{\mathcal{R}}_{km}\eta_m^{(\alpha)}\eta_l^{(\alpha)} V^{(\alpha)} = \bar{\mathcal{R}}_{km} \left\{ \frac{1}{\mathcal{V}} \sum_{\alpha=1}^{N} \eta_m^{(\alpha)}\eta_l^{(\alpha)} V^{(\alpha)} \right\} = \bar{\mathcal{R}}_{km}\delta_{ml} = \bar{\mathcal{R}}_{kl}. \tag{120}$$

Using the definitions in equations (117), (118), (119), and (120), equation (115) for the continuum model can be written

$$\bar{\mathcal{M}}_{kl} = (\bar{e}_{kl} - \bar{\Phi}_{kl}) + [\bar{r}_{kl} - \bar{\mathcal{R}}_{kl}], \tag{121}$$

where the terms in the parentheses (…) constitute the isochoric macrostrain and the terms in brackets […] constitute the relative rotation. We can also write the left-hand side of equation (121) in terms of the transpose of the moment tensor:

$$\bar{\mathcal{M}}_{kl}^{\mathrm{T}} = \bar{\mathcal{M}}_{lk} = (\bar{e}_{lk} - \bar{\Phi}_{lk}) + [\bar{r}_{lk} - \bar{\mathcal{R}}_{lk}]. \tag{122}$$

Using the symmetry of $\bar{e}_{lk}$ and $\bar{\Phi}_{lk}$ (equations 104 and 118) and the antisymmetry of $\bar{r}_{lk}$ and $\bar{\mathcal{R}}_{lk}$ (equation 104), we have

$$\bar{\mathcal{M}}_{kl}^{\mathrm{T}} = (\bar{e}_{kl} - \bar{\Phi}_{kl}) + [\bar{\mathcal{R}}_{kl} - \bar{r}_{kl}]. \tag{123}$$

Equation (123) is the same as the micropolar moment-density tensor for the discrete-block model (equation 102). Thus, the continuum and the discrete-block models give identical results for the volume-averaged quantities, because

$$\bar{e}_{kl} = e_{kl}, \qquad \bar{\Phi}_{kl} = \Phi_{kl}, \qquad \bar{r}_{kl} = r_{kl}, \qquad \bar{\mathcal{R}}_{kl} = \mathcal{R}_{kl}. \tag{124}$$

Relation of the Continuum Relative Vorticity Parameter to the Micropolar Moment-Density Tensor. In the continuum micropolar model, the relative vorticity parameter vector is defined as

$$\bar{W}_k \equiv \frac{\varepsilon_{kml}(\hat{\bar{\omega}}_{lm} - \hat{\bar{w}}_{lm})}{\hat{\bar{d}}_1 - \hat{\bar{d}}_3} \tag{125}$$

(Twiss *et al.*, 1991, equation 10.2; Twiss *et al.*, 1993, equation 10), where $\bar{\boldsymbol{\omega}}$ is the microvorticity tensor, $\bar{\mathbf{w}}$ is the macrovorticity tensor, and $\bar{\mathbf{d}}$ is the deformation rate tensor. $\bar{\mathbf{d}}$ and $\bar{\mathbf{w}}$ are, respectively, the symmetric and antisymmetric parts of the macrovelocity gradient tensor. The circumflex (hat) on the variables indicates that the components are given in the principal coordinates of the deformation rate tensor $\bar{\mathbf{d}}$. In applications, we have used only the component of this vector parallel to the $\hat{\bar{d}}_2$ principal axis, which we refer to as the relative vorticity parameter,

$$\bar{W} = \bar{W}_2 \equiv \frac{\varepsilon_{2ml}(\hat{\bar{\omega}}_{lm} - \hat{\bar{w}}_{lm})}{\hat{\bar{d}}_1 - \hat{\bar{d}}_3} = \frac{(\hat{\bar{\omega}}_{13} - \hat{\bar{w}}_{13})}{0.5(\hat{\bar{d}}_1 - \hat{\bar{d}}_3)}. \tag{126}$$

The relative vorticity parameter is defined in terms of the rates of the kinematic variables. Thus, if we multiply the top and bottom of equations (125) and (126) by dt, we can convert the definition to the instantaneous kinematic variables, as defined in equation (104):

$$\bar{W}_k \equiv \frac{\varepsilon_{kml}(\hat{\bar{\omega}}_{lm} - \hat{\bar{\omega}}_{lm})dt}{(\hat{\bar{d}}_1 - \hat{\bar{d}}_3)dt},$$

$$\bar{W}_k = \frac{\varepsilon_{kml}(\hat{\bar{\mathcal{R}}}_{lm} - \hat{\bar{r}}_{lm})}{(\hat{\bar{e}}_1 - \hat{\bar{e}}_3)}, \qquad \bar{W} = \frac{(\hat{\bar{\mathcal{R}}}_{13} - \hat{\bar{r}}_{13})}{0.5(\hat{\bar{e}}_1 - \hat{\bar{e}}_3)}. \tag{127}$$

Using equation (124), the relations for the relative vorticity parameter in equation (127) can be written in terms of variables derived for the discrete-block model as

$$\bar{W}_k = \frac{\varepsilon_{kml}(\hat{\mathcal{R}}_{lm} - \hat{r}_{lm})}{(\hat{e}_1 - \hat{e}_3)}, \qquad \bar{W} = \frac{(\hat{\mathcal{R}}_{13} - \hat{r}_{13})}{0.5(\hat{e}_1 - \hat{e}_3)}, \tag{128}$$

where the superposed circumflex indicates components in the principal coordinates of the macrostrain e_{kl}, which is defined for the discrete-block model by equation (38) with (44).

We can now examine how the results in equations (127) and (128) are related to the micropolar moment-density tensor for the discrete-block model. The axial vector associated with the antisymmetric part of this moment tensor is given by

$$\varepsilon_{kji}\hat{\mathcal{M}}^{\mathrm{T}}_{ij} = \varepsilon_{kji}(\hat{e}_{ij} - \hat{\Phi}_{ij}) + \varepsilon_{kji}[\hat{\mathcal{R}}_{ij} - \hat{r}_{ij}].$$

Because $(\hat{e}_{ij} - \hat{\Phi}_{ij})$ is symmetric with respect to ij and ε_{kji} is antisymmetric with respect to ij,

$$\varepsilon_{kji}\hat{\mathcal{M}}^{\mathrm{T}}_{ij} = \varepsilon_{kji}[\hat{\mathcal{R}}_{ij} - \hat{r}_{ij}]. \tag{129}$$

Thus, from equations (128) and (129) the relative vorticity parameter vector is related to the moment tensor by

$$\bar{W}_k = \frac{\varepsilon_{kji}\hat{\mathcal{M}}^{\mathrm{T}}_{ij}}{(\hat{e}_1 - \hat{e}_3)}. \tag{130}$$

This same relationship also holds if we rewrite equation (130) using the equivalent variables from the continuum micropolar model, because the micropolar moment density and the strain tensors for the discrete-block model and the continuum model are equivalent (equations 102, 123, and 124).

Thus, the relative vorticity parameter vector is the axial vector defined from the antisymmetric part of the transposed micropolar moment-density tensor, normalized by the maximum instantaneous shear, where the components are specified in the principal coordinates of the instantaneous macrostrain e_{kl}.

For the second component of the relative vorticity parameter vector, setting $k = 2$ in equation (130), we have for the discrete-block model

$$\bar{W} = \bar{W}_2 = \frac{\varepsilon_{2ji}\hat{\mathcal{M}}^{\mathrm{T}}_{ij}}{(\hat{e}_1 - \hat{e}_3)} = \frac{\hat{\mathcal{M}}^{\mathrm{T}}_{13} - \hat{\mathcal{M}}^{\mathrm{T}}_{31}}{(\hat{e}_1 - \hat{e}_3)} = \frac{0.5(\hat{\mathcal{M}}^{\mathrm{T}}_{13} - \hat{\mathcal{M}}^{\mathrm{T}}_{31})}{0.5(\hat{e}_1 - \hat{e}_3)}. \tag{131}$$

Evidence for Nonrecoverable Micropolar Effects

I and my colleagues Jeffrey Unruh and Jonathan Lewis have studied the seismogenic strain in numerous seismically active areas by inverting seismic focal mechanisms and fault-slickenline data using the computer program FLTSLP (written by Twiss and Guenther), which incorporates the micropolar theory in the inversion. An inversion solution consists of the orientation of the principal strain rate axes $\hat{d}_k$, or equivalently the principal instantaneous strain axes $\hat{e}_k$; their relative magnitudes given by the deformation rate parameter, or equivalently the instantaneous strain parameter D,

$$D \equiv \frac{\hat{d}_2 - \hat{d}_3}{\hat{d}_1 - \hat{d}_3} = \frac{\hat{e}_2 - \hat{e}_3}{\hat{e}_1 - \hat{e}_3}; \tag{132}$$

and the relative vorticity parameter, or equivalently the relative instantaneous rotation parameter (W), which are defined, respectively, in equations (126) and (128). For convenience, we drop the overbar notation in this section as we have shown that the distinction between the micropolar continuum model and the discrete-block model is no longer required.

Our inversions very commonly give nonzero values of the relative vorticity parameter W that are statistically significant at the 95% confidence level. This parameter, therefore, appears to reflect a real kinematic characteristic of the seismogenic deformation, which we interpret to be the independent rotations of the fault blocks in the fault zone. We have searched specifically for areas in which we can make independent tests of the inferred block rotations, and we review here results from three such areas in California (Fig. 4). These areas, all of which are dominated by dextral strike-slip faulting, are the 1992 Landers earthquake aftershock sequence in the eastern California shear zone in the Mojave desert (Unruh *et al.*, 1996); the 1989 Loma Prieta earthquake aftershock sequence along the San Andreas fault in the Santa Cruz Mountains south of San Francisco Bay (Twiss and Unruh, 2007); and the deformation in the Coso Range east of the Sierra Nevada between Owens Valley and the Garlock fault (Lewis *et al.*, 2007).

Individually, the results from these three studies do not provide conclusive proof of the theory. This is in part because of the lack of quantitative data that permit an independent determination of the relative vorticity parameter and in part because of the insufficient resolution of available quantitative data. Taken together, however, the consistency of the results from all these studies with the micropolar model provides stronger support for the theory than any of the results considered separately. I briefly describe these three examples in turn.

The 1992 Landers Earthquake Aftershock Sequence

Unruh *et al.* (1996) inverted clusters of aftershock focal mechanisms from the 1992 Landers earthquake zone (Fig. 4). The inversion for aftershocks along the Kickapoo

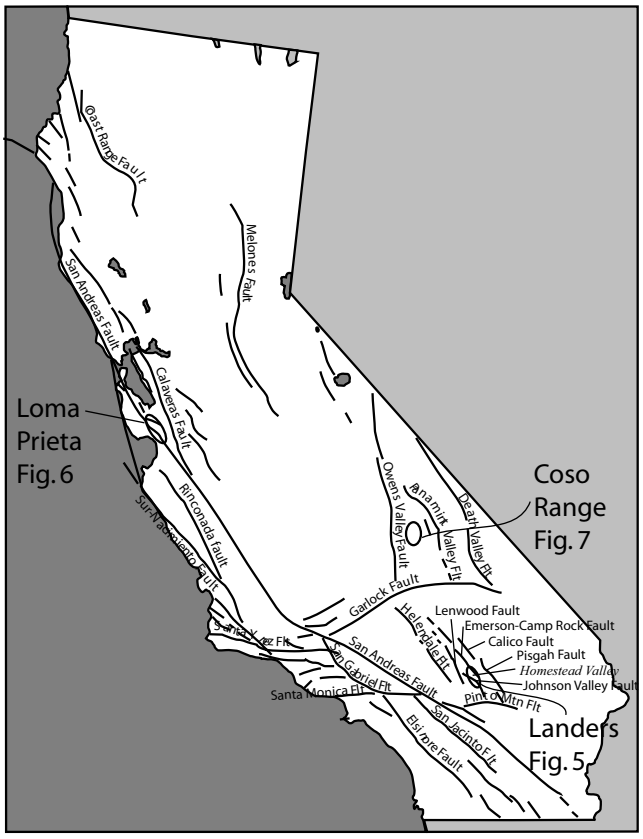

Figure 4. Index map of California faults highlighting the locations of the 1992 Landers aftershocks, the 1989 Loma Prieta aftershocks, and the Coso Range, as discussed in the text (see the Data and Resources section).

fault (Fig. 5) gave values for the instantaneous strain parameter $D = 0.5$, implying a plane strain, and for the relative rotation parameter $W = 0.4$ about a positive-down axis (Fig. 5a). Subsequent to our analysis of the Landers aftershocks, we added to our inversion program the capability of evaluating the confidence limits for the inversion parameters. Inversions of focal mechanisms from other areas suggest that the 95% confidence level for D and W are, respectively, approximately ± 0.15 and ± 0.3 (e.g., Twiss and Unruh, 2007, fig. 11B). Thus, we infer that the value of W on the Kickapoo fault is significantly different from zero. For a dextral shear zone such as is represented by these faults, the macrorotation is positive about a positive-down axis (clockwise looking down). A positive value of the relative rotation parameter then implies that the clockwise rotation of the fault blocks exceed the macrorotation associated with the macroshear along the faults.

The results for the relative rotation parameter can be compared with the geometry and kinematics of fault blocks in the fault zones based on mapping of surface fractures. In Homestead Valley, Sowers *et al.* (1994) mapped shear zones and zones of extension fractures trending roughly north–south to northeast–southwest within a 2.5 km wide stepover between the Johnson Valley fault to the south and the Homestead Valley fault to the north (Fig. 5b). The stepover is bounded on the northwest side by the Kickapoo fault and on the southeast side by a northeast–southwest trending zone of surface fractures (Fig. 5). Near the Johnson Valley fault is a 1 km wide zone of shearing including a number of distinct shear zones. The kinematic significance of these structures is suggested by similar structures having a scale of up to tens of meters, mapped by Johnson *et al.* (1993) along both the Johnson Valley fault and the Homestead Valley fault. They showed that north-northeast trending fractures had sinistral offset, and they inferred that the surface fractures and kinematic indicators implied a clockwise-looking-down rotation of the fault blocks within the shear zones, as well as a component of extension normal to the dextral faults.

The ground-based mapping can be compared with the results of the inversion of the aftershock focal mechanisms if we assume that the geometry and kinematic significance of the surface fractures reflects that of the faults at the depths of the inverted aftershocks. For the observed angle $\alpha \approx 135°$ to 150° between the long dimension of the rotating blocks and the shear zone (Fig. 5b,c), a pinned-block model of fault blocks rotating in a shear zone (Twiss *et al.*, 1993) gives values of the instantaneous strain parameter D and the relative rotation parameter W of $(D, W) = (0.36, 0.45)$ and (0.44, 0.28), respectively (Fig. 5a). These values are consistent (within the inferred confidence limits) with the inversion solution for the aftershocks along the Kickapoo fault (Fig. 5a).

Despite the consistency between the results from the inversion of aftershock focal mechanisms and the geometry and kinematics of the mapped faults, the conclusiveness of these results as a test of the micropolar theory has two limitations. First, independent quantitative measures of the macrorotation and the microrotation are not available, so an independent value of the relative vorticity cannot be determined. Second, although the pinned-block model for fault-block rotation in a shear zone provides the best fit of the models considered by Twiss *et al.* (1993) and Unruh *et al.* (1996), the pinned-block model for block rotation is not unique, and there are no independent constraints on what the most appropriate model should be.

Loma Prieta Aftershock Sequence

Twiss and Unruh (2007) made a detailed study of the aftershock sequence of the 1989 Loma Prieta earthquake, which occurred along the San Andreas fault system in central California (Figs. 4 and 6a). We divided the focal mechanisms for over 1100 aftershocks into 17 volumetrically defined clusters and subdivided these clusters into a total of 34 subsets, defined by the requirement that each subset reflect a homogeneous deformation. The inversions provided the orientations of the principal instantaneous strains, their relative magnitudes as defined by the instantaneous strain parameter D, and the instantaneous relative rotation parameter W measured about the intermediate principal strain axis. The kine-

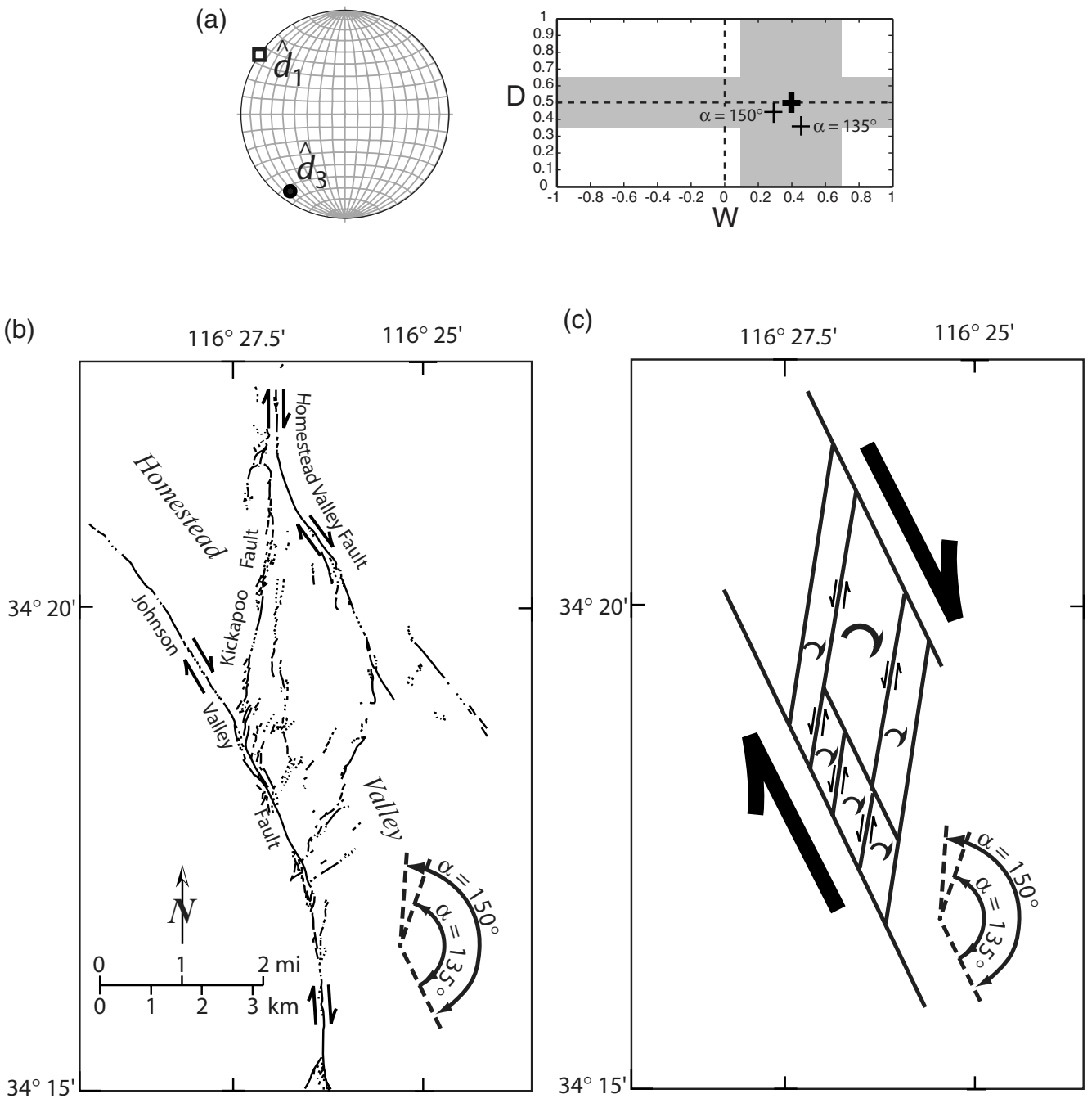

Figure 5. Part of the fault system involved in the 1992 Landers earthquake. (a) Micropolar solution for the Kickapoo fault. The stereogram shows the aftershock inversion solution for the orientation of the principal lengthening ($\hat{d}_1$) and shortening ($\hat{d}_3$) axes (lower hemisphere, equal area projection). The graph shows solutions for the relative instantaneous rotation parameter W versus the instantaneous deformation parameter D. The black plus indicates the value inferred from inversion of aftershocks along the Kickapoo fault. The gray bands (after Twiss and Unruh, 2007) illustrate the probable 95% confidence limits. The fine plus marks show the values of D and W calculated from the pinned-block model of Twiss *et al.* (1993) for the observed angle α between the shear zone and the fault blocks. (b) Geometry of fault blocks in part of the aftershock zone near the intersection of the Kickapoo, Johnson Valley, and Homestead Valley faults (after Sowers *et al.* [1994] and Unruh *et al.* [1996]). The fault blocks in the stepover between the Johnson Valley fault and the Homestead Valley fault make an angle $\alpha \approx$ 135° to 150° with the shear zone boundary. (c) A highly idealized model of fault blocks in the map in part (b). The stepover is in a dextral fault system. Clockwise rotation of the fault blocks in the stepover requires sinistral slip on the north-northeast striking faults.

matic environment for the aftershock zone as a whole is a convergent dextral strike slip, with strike slip dominant in the southern part of the aftershock zone, dextral-reverse slip dominant in the northern part, and reverse slip dominant in a shallow zone above about 5 km depth, which is above the upper tip line of the main fault.

The principal axes of instantaneous shortening $\hat{e}_3$ are oriented north-northeast–south-southwest subhorizontal for

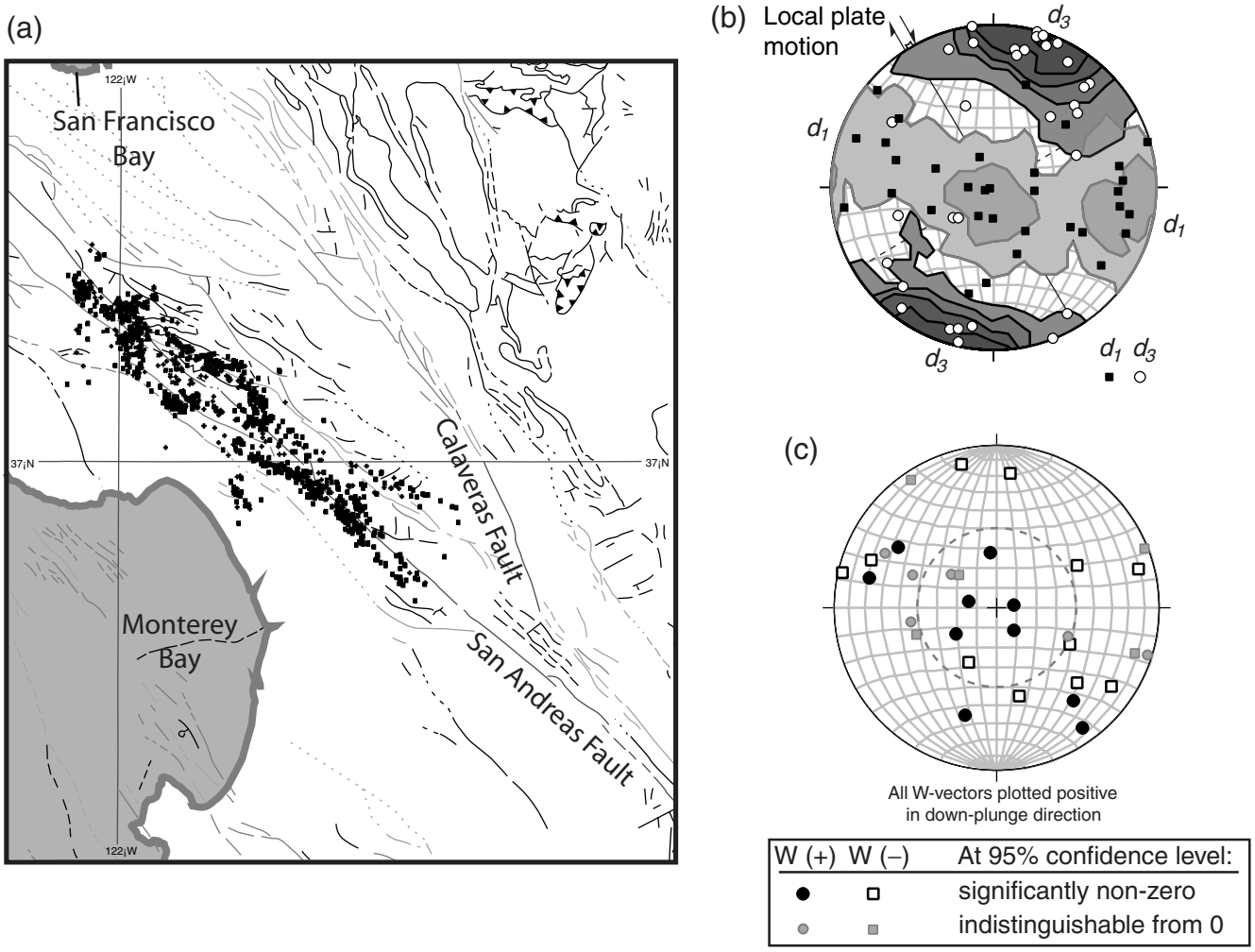

Figure 6. 1989 Loma Prieta fault aftershock sequence (after Twiss and Unruh, 2007). (a) Location map showing the epicenters for more than 1100 aftershocks for which focal mechanisms are available. The faults on the base map are taken from Jennings and Saucedo (1994). (b) Collected solutions to subsets showing the point maximum for the axes of maximum shortening $\hat{d}_3$, and the girdle normal to that maximum for the axes of maximum lengthening $\hat{d}_1$. Lower hemisphere, equal area projection with Kamb contours at intervals of 2σ above uniform. (c) Magnitudes of the relative instantaneous rotation parameter W parallel to the axis of intermediate principal instantaneous strain $\hat{d}_2$, plotted as positive-down. Positive, near-zero, and negative values of W are distinguished by symbol and fill color. For vectors that have a plunge steeper than 50° (within the dashed small circle) and a significantly nonzero value of W, the sign of W is positive for five out of six. Lower hemisphere, equal area projection.

most of the inversion solutions (Fig. 6b). The principal axes of instantaneous lengthening $\hat{e}_1$ define a girdle normal to the common shortening axis with weak maxima in the girdle that are oriented subhorizontal and subvertical. The solutions for which the principal shortening and lengthening axes are both subhorizontal, reflect dominantly dextral strike slip on the faults and, therefore, a positive (clockwise) macrorotation about a positive-down intermediate principal axis. For those solutions with an intermediate principal axis plunging at greater than 50°, six have a value of the relative rotation parameter that is nonzero at the 95% confidence level. Of these six, five have a positive value of W (Fig. 6c).

Dextral strike slip is the dominant macroshear along this fault, and it is therefore associated with a steeply plunging intermediate principal strain axis. Thus, we would expect the instantaneous relative rotation parameters W to be most consistent for solutions having a steeply plunging intermediate principal strain axis. The results (Fig. 6c) show the expected consistency and indicate that block rotation of fault blocks in the shear zone generally exceeds the macrorotation of the dextral shear in the macrocontinuum.

This consistency supports the micropolar model of block rotation in the shear zone, but because we do not have the information to determine independently the instantaneous relative rotation parameter W or the fault block geometry, the consistency provides only permissive, but not conclusive, support for the theory.

Coso Geothermal Area

The Coso Range in east central California south of the Owens Valley (Figs. 4 and 7a) has provided us with the best

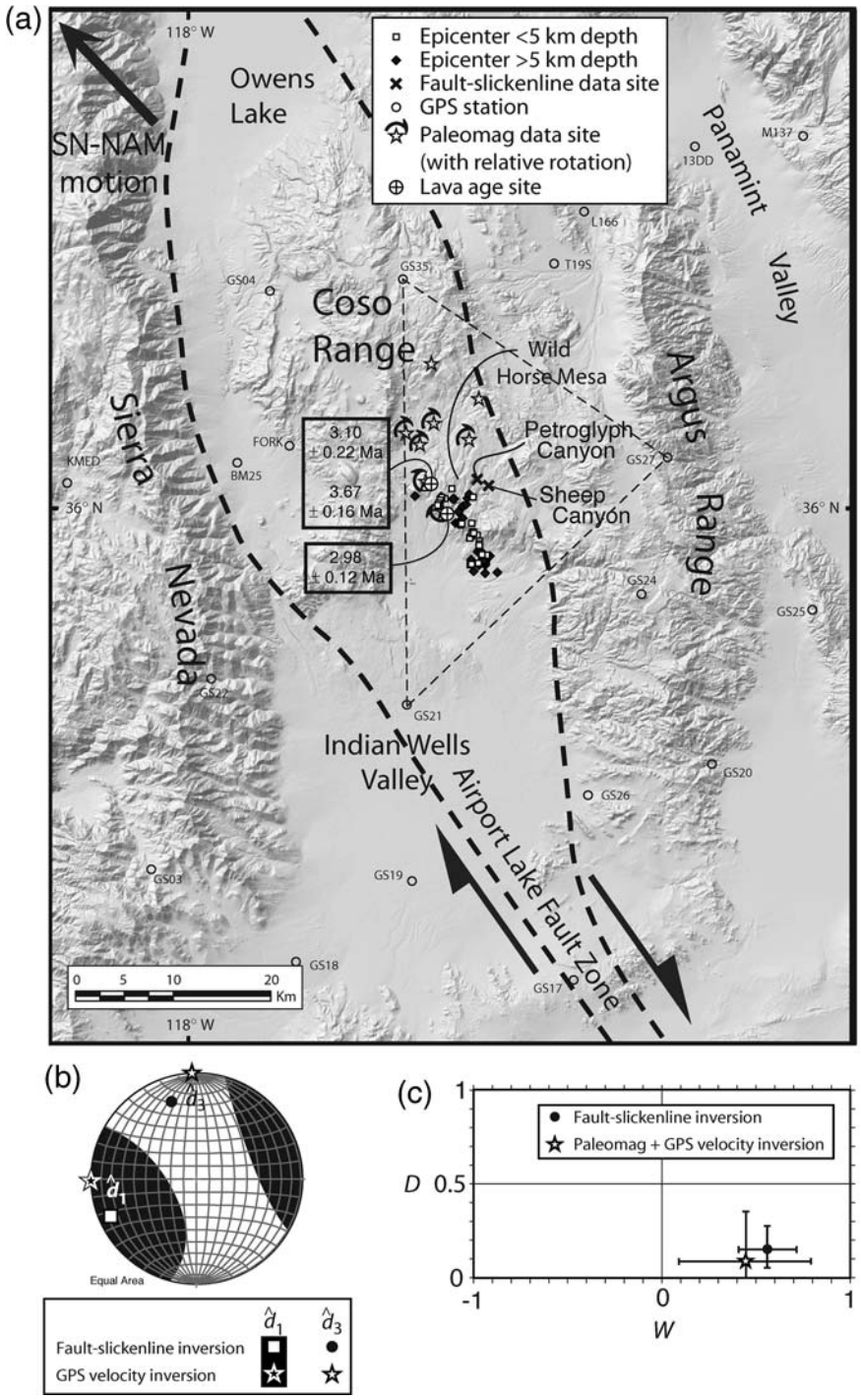

Figure 7. Coso Range (after Lewis *et al.* [2007]). (a) Map showing the location of the Coso Range in east central California and of Wild Horse Mesa within the Coso Range. Labeled open dots are the GPS stations of McClusky *et al.* (2001). The triangle with vertices at three of the GPS stations is cell 34 of Lewis *et al.* (2007), which includes Wild Horse Mesa. The letter X labels the locations in Petroglyph Canyon and Sheep Canyon where the fault-slickenline data were gathered. Stars show locations from which the paleomagnetic orientations were determined; curved arrows around the stars show the paleomagnetic rotation of lavas in the fault stepover relative to the same lavas outside the stepover, which averages $12.0° \pm 2.6°$. Solid diamonds and open squares show the epicenters of earthquakes at greater than and less than 5 km depth, respectively; the focal mechanisms from these events were inverted for a solution of the local deformation. (b) Stereogram showing the orientations of the axis of maximum rates of lengthening ($\hat{d}_1$) and shortening ($\hat{d}_3$) inferred from the inversion of fault-slickenline data and from the inversion of GPS velocity data from the triangular cell shown in part (a). The boundary of the shaded areas is the locus of zero instantaneous extension. Lower hemisphere equal area projection. (c) Values of the deformation rate parameter D and the relative vorticity parameter W inferred from two independent methods: first, from the inversion of fault-slickenline data; and second, from the inversion of GPS velocities for the vertices of the triangular cell in part (a), which defines the macrovorticity and the maximum macroshear rate, and from the paleomagnetically determined block-rotation rates, which define the microvorticity.

opportunity that we have found to do an independent test of the micropolar interpretation of block rotation in a shear zone. The area is an active geothermal area that lies within the China Lake Naval Weapons Station. The geothermal energy powers an electrical power generation plant, and the Geothermal Program Office of the U.S. Navy, until recently headed by Frank Monastero, has sponsored a remarkable series of studies to improve the understanding and management of the geothermal resource.

Among the many studies of the Coso area have been Global Positioning System (GPS) studies of the displacements in a network of stations that span the Coso Range (Fig. 7a, McClusky *et al.*, 2001); studies of the paleomagnetism recorded by multiple flows of young lavas in the Coso Range (e.g., Pluhar, 2003; Pluhar *et al.*, 2005); geochronology of the lavas (Duffield *et al.*, 1980; Pluhar, 2003; Pluhar *et al.*, 2005); seismic studies, which have produced a large catalog of focal mechanisms (e.g., Hauksson, 2000); and field studies of fault-slickenline data (Lewis *et al.*, 2007).

Lewis *et al.* (2007) undertook a comparison of the deformations inferred from these different sources of data for an area that is centered on Wild Horse Mesa in the Coso Range (Fig. 7a). This area lies in a right stepover in a dextral fault system, and it is characterized by a system of elongate fault blocks bounded by normal faults. In principle, a complete independent test of the micropolar inversion solutions for either the focal mechanism data or the fault-slickenline data is possible by using the GPS studies to define the macrostrain rate and the macrovorticity and by using the paleomagnetism with the geochronology to define the microvorticity for the block rotations. The value of D can be calculated from the principal values of the macrostrain rate (equation 132), and the value of W can be calculated from the difference between the microvorticity and the macrovorticity, normalized by the maximum shear rate (equation 126).

To apply the test, two assumptions are fundamental: first, the GPS data, the micropolar inversions of both focal mechanisms and fault-slickenline data, and the paleomagnetically defined rotations all must describe aspects of the same deformation, and second, the deformation rate must be steady across the time spans over which the average rates for the different measurements are determined. These time spans vary from a few years or less, which is the time typically taken to accumulate both the GPS measurements and the catalog of seismic events, to times of up to 2 or 3 Ma, which is the time over which the paleomagnetically determined rotations have accumulated and presumably the time during which the fault slickenlines developed.

Inversions of the focal mechanisms define two distinct solutions that separate the seismic events into a shallow zone above 5 km depth, in which faulting is dominantly normal faulting, and a deeper zone between 5 and 8 km, in which faulting is dominantly dextral strike slip. The two solutions share a common orientation of the maximum extension $\hat{e}_1$ of about [plunge, trend] = [15°, 257°] (68% confidence limits ≈10°). Inversions of the fault-slickenline data define three different solutions; of the three, the most well defined is predominantly dextral strike slip with a component of vertical shortening (crustal thinning). The orientation of $\hat{e}_1$ is [12°, 246°] (68% confidence limits ≈11°, Table 2), very similar to the focal mechanism inversion solutions. The other two fault-slickenline solutions are a normal faulting and a thrust faulting, neither of which is as well defined as the strike-slip solution.

The deformation was determined independently from the GPS data by dividing the area into a network of cells using the GPS stations as the vertices. The measured velocities at the vertices were then inverted for the strain rate and rotation rate within each cell. The principal strain rates are presumed to be horizontal and vertical, and the vertical component is determined from the measured horizontal components assuming a constant-volume deformation. The GPS solution for the Wild Horse Mesa area was obtained by inverting the GPS velocities from the triangular cell that includes Wild Horse Mesa near its center (Fig. 7a, cell 34 of Lewis *et al.*, 2007). The solution shows a dominantly dextral strike-slip deformation (Fig. 7b) with $\hat{e}_1$ oriented [00°, 269°] (68% confidence limits = 6°) and with a component of crustal thinning ($D = 0.09 + 0.27/-0.09$, Table 2; Fig. 7c). Because this cell is large relative to the fault blocks in the mesa, this solution defines the macrostrain rate and macrovorticity for the area.

Table 2

Test of the Fault-Slickenline Inversion Solution with GPS and Paleomagnetic Data for the Wild Horse Mesa Area in the Coso Range, East-Central California (from Lewis *et al.*, 2007)

	Fault-Slickenline Inversion Solution*	GPS/Paleomag Solution†
$\hat{d}_1$ [plunge, trend]	[12°, 246°] (12°; 10°)	[00°, 269°] (6°)
$\hat{d}_2$ [plunge, trend]	[62°, 132°]	[90°, 000°]
$\hat{d}_3$ [plunge, trend]	[24°, 343°] (38°; 6°)	[00°, 359°] (6°)
D	0.15 (+0.13; −0.10)	0.09 (+0.27/ − 0.09)
W	0.56 (+0.16; −0.15)	0.44 (±0.35)

*Error (given in parentheses) is the maximum and minimum deviation of the 68% confidence limit from the solution, based on the solutions to 2000 bootstrap data sets.

†Error (given in parentheses) is the 68% confidence limit.

The microrotation in the shallow crust within the fault stepover is defined by the paleomagnetic rotation of the lavas in the fault blocks on Wild Horse Mesa (Fig. 7a) relative to the same lavas outside the fault stepover. The paleomagnetic data represent a cumulative relative rotation of $12.0° \pm 2.6°$ (6% confidence limits) over a period of at most 3.5 Ma, which is the maximum age of the lavas. The actual duration of the deformation associated with the rotations, however, is not well constrained, although Monastero *et al.* (2002) have proposed that the divergent dextral shearing could have started as late as 2 Ma. Thus, the microvorticity calculated using the paleomagnetic rotation and the age of the lavas is subject to considerable uncertainty.

The inversion solutions from the seismic focal mechanism data cannot be tested directly against the GPS and paleomagnetic data. For the focal mechanisms below 5 km depth, the deformation is dextral strike-slip faulting like the GPS solution. But, the geometry of the fault structures is not known, and there are no independent data that determine the kinematics of block rotation. Thus, the microrotation, and thereby the relative vorticity parameter W, cannot be determined independently of the focal mechanism inversion solution. For the focal mechanisms above 5 km depth, the inversion solution shows normal faulting, which presumably reflects the edge effects above the blind strike-slip fault below 5 km depth (Bowman *et al.*, 2003). This solution, however, reflects only a subordinate part of the dominantly dextral strike-slip GPS solution. Thus, the two solutions are not directly comparable.

The strike-slip solution from the inversion of the fault-slickenline data is most comparable to the dextral strike-slip solution from the GPS velocity data. Both these data sets, as well as the paleomagnetic data, characterize the deformation of the shallow crust. The GPS data define the macrostrain rate and macrovorticity, and the paleomagnetic data with the age limits define the microvorticity. Thus, in principle, from these data we can determine a complete and independent micropolar solution for the deformation, which we can use to test the inversion solution from the fault-slickenline data and the micropolar model of block rotations.

The slickenlines and the paleomagnetic rotations reflect a permanent deformation that developed during faulting over an imperfectly known span of time of between 2 and 3.5 Ma, whereas the GPS data reflect a geologically instantaneous deformation that presumably includes both permanent and elastic components. Therefore, in comparing the fault-slickenline inversion results with the characteristics of deformation obtained from the GPS studies and the paleomagnetic data, we must assume that the deformation rate has been steady from 2 or 3 Ma through to the present day and that any elastic component in the GPS deformation will ultimately be converted to a permanent deformation.

Given these caveats, and assuming the 2 Ma onset of divergent dextral shear in the area (Monastero *et al.*, 2002), we find that the results for the fault-slickenline inversions and the GPS solutions, respectively, are very similar (Table 2, Fig. 7b,c). In particular, the value of the relative vorticity parameter W determined from inverting the fault-slickenline data is consistent with the value determined independently from the GPS and paleomagnetic data, which would seem to confirm the micropolar theory.

This favorable comparison, however, reflects choices (including the time span for the accumulation of the paleomagnetic rotation and the specific cell for which the GPS solution was calculated) that, although justifiable, are not unique. Other assumptions lead to less convincing or even contradictory results (Lewis *et al.*, 2007, tables 1–4). This analysis also depends on the assumption that it is appropriate to compare the fault-slickenline inversion solution for dextral strike slip with the GPS solution and to combine the rates of deformation determined from the short-time-span GPS data with the rotation rates determined from the long-time-span paleomagnetic data. Given these caveats, the independent support for the micropolar theory is encouraging but not definitive (see the discussion in Lewis *et al.*, 2007).

Conclusions

I derive an objective asymmetric micropolar moment tensor from a discrete-block model for a deforming granular material. This moment tensor is a generalization of the standard symmetric seismic moment tensor. The definition used here is for a geometric moment tensor, which does not include the shear modulus that is usually included in the seismic moment tensor. Thus, the micropolar moment tensor reflects the deformation in the material rather than the inferred stress.

In a micropolar material, which is composed of rigid blocks or grains, two independent components of deformation coexist. The first component is the centroid deformation, which is defined by the motions of the block centroids. Taking a moving average of the centroid motions over a sufficiently large volume defines a continuum field of the macrodeformation. The second component of the deformation is the rigid rotation of the blocks about their centroids. A moving average of these rotations over a sufficiently large volume defines a continuum field of the microrotation. Both the centroid deformation and the block rotation contribute to slip on shear planes, which are the interfaces between adjacent blocks.

I derive the separate contributions of the centroid deformation and the block rotation to the local micropolar moment tensor for individual slip events. Combining these contributions defines the complete local micropolar moment tensor for individual slip events. I also define the separate contributions of the macrodeformation and the microrotation to the micropolar moment-density tensor for clusters of slip events in a volume that is large relative to the block size. Then combining these separate averaged deformations defines the complete micropolar moment-density tensor.

Both the local micropolar moment tensor and the micropolar moment-density tensor describe an isochoric (constant-

volume) deformation, which is defined as the total deformation minus an anisotropic volumetric deformation. The isochoric deformation reduces to the deviatoric deformation if the volumetric deformation is isotropic.

The symmetric part of the local micropolar moment tensor depends not only on the local centroid deformation but also on the local block rotation. This demonstrates that an inversion of a set of seismic focal mechanisms, each of which reflects a classical symmetric seismic moment tensor, can be used to infer constraints on the microrotation.

In a granular material, the moment of momentum is not balanced locally as in classical theory but is balanced on the scale of the rigid blocks that define the substructure of the material. Thus, any individual slip event is treated as a single-couple, not a double-couple, mechanism. The antisymmetric part of the local micropolar moment tensor arises from the difference between the rotation of the blocks about their centroids and the independent rotation associated with the shear that results from the local centroid displacement gradient. The antisymmetric part of the micropolar moment-density tensor arises from the difference between the microrotation and the macrorotation, the latter being a part of the macrodeformation. The difference between the two rotations is independent of the rotation of any coordinate system in which the tensors are described, so the local micropolar moment tensor and the micropolar moment-density tensors are objective quantities.

This discrete-block model results in the equations for seismogenic strain similar to those found by Kostrov (1974). When the deformation in the descrete-block model, which occurs on individual slip planes, is averaged over a volume that is large with respect to the size of the blocks, the resulting equations are essentially the same as those developed from the continuum micropolar theory by Twiss and coworkers (Twiss *et al.*, 1991, 1993; Twiss and Unruh, 1998). The analysis here also defines the explicit relationship between the instantaneous relative rotation parameter W, which was defined for the continuum micropolar theory, and the antisymmetric part of the micropolar moment-density tensor.

I review briefly three investigations of the seismogenic deformation associated with volumes of distributed seismicity in three different areas. The results from these investigations support the micropolar model for the effects of a granular substructure on the characteristics of seismic focal mechanisms. Individually, these results do not provide definitive tests, either because quantitative data are unavailable by which we could calculate the micropolar parameters independently of the inversion of the focal mechanism data, or because the independent quantitative data are of insufficient resolution. Collectively, however, the consistency of the results with the predictions of the theory seems to favor the micropolar interpretation for the origin of the antisymmetric component of the micropolar moment tensor.

Data and Resources

All data used in this article came from published sources listed in the references. The base map used in Figure 4 was modified from the U.S. Geological Survey Web site (http://education.usgs.gov/california/maps/faults_names1.htm, last accessed February 2009).

Acknowledgments

The reviews by two anonymous reviewers are gratefully acknowledged.

References

Bowman, D., G. King, and P. Tapponnier (2003). Slip partitioning by elastoplastic propagation of oblique slip at depth, *Science* **300,** 1121–1123.

Cosserat, E., and F. Cosserat (1909). Théorie des corps déformables, in *Traité de Physique*, Second Ed., O. D. Chwolson (Editor), Vol. **2**, Hermann, Paris, 953–1173.

Duffield, W. A., C. R. Bacon, and G. B. Dalrymple (1980). Late Cenozoic volcanism, geochronology, and structure of the Coso Range, Inyo County, California, *J. Geophys. Res.* **85,** 2381–2404.

Eringen, A. C. (1966a). Linear theory of micropolar elasticity, *J. Math. Mech.* **15,** no. 6, 909–924.

Eringen, A. C. (1966b). Theory of micropolar fluids, *J. Math. Mech.* **16,** no. 1, 1–18.

Eringen, A. C. (1999a). *Microcontinuum Field Theories I: Foundations and Solids*, Springer, New York, 325 pp.

Eringen, A. C. (1999b). *Microcontinuum Field Theories II: Fluids*, Springer, New York.

Hauksson, E. (2000). Crustal structure and seismicity distribution adjacent to the Pacific and North America plate boundary in southern California, *J. Geophys. Res.* **105,** 13,875–13,903, doi 10.1029/2000JB900016.

Jackson, J., and D. McKenzie (1988). The relationship between plate motions and micropolar moment tensors, and the rates of active deformation in the Mediterranean and Middle East, *Geophys. J.* **93,** 45–73.

Jennings, C. W., and G. J. Saucedo (1994). Fault activity map of California and adjacent areas, California Department of Conservation, Division of Mines and Geology, California Geologic Data Map Series, Map No. 6, scale 1:750,000.

Johnson, A. M., R. W. Fleming, and K. M. Cruikshank (1993). Broad belts of shear zones as the common form of surface rupture produced by the 28 June 1992 Landers, California earthquake, *U.S. Geol. Surv. Open-File Rept. 93–348*.

Julian, B. R., A. D. Miller, and G. R. Foulger (1998). Non-double-couple earthquakes 1. Theory, *Rev. Geophys.* **36,** no. 4, 525–549.

Kostrov, V. V. (1974). Seismic moment and energy of earthquakes, and seismic flow of rock, *Acad. Nauk. SSSR Phys. Solid Earth* **1,** 13–21.

Lewis, J. C., R. J. Twiss, C. J. Pluhar, and F. C. Monastero (2007). Multiple constraints on divergent strike-slip deformation along the eastern margin of the Sierran microplate, SE California in *Exhumation Associated with Continental Strike-Slip Systems*, GSA Special Paper 434 A. B. Till, S. M. Roeske, J. C. Sample, and D. A. Foster (Editors), Geological Society of America, Boulder, Colorado, 107–128.

McClusky, S. C., S. C. Bjornstad, B. H. Hager, R. W. King, B. J. Miller, F. C. Monastero, and B. J. Souter (2001). Present day kinematics of the eastern California shear zone from a geodetically constrained block model, *Geophys. Res. Lett.* **28,** no. 17, 3369–3372, doi 10.1029/2001GL013091.

Miller, A. D., G. R. Foulger, and B. R. Julian (1998). Non-double-couple earthquakes 2. Observation, *Rev. Geophys.* **36,** no. 4, 551–568.

Molnar, P. (1983). Average regional strain due to slip on numerous faults of different orientations, *J. Geophys. Res.* **88,** 6430–6432.

Molnar, P., and Q. Deng (1984). Faulting associated with large earthquakes and the average rate of deformation in central and eastern Asia, *J. Geophys. Res.* **89,** no. B7, 6203–6227.

Monastero, F. C., J. D. Walker, A. M. Katzenstein, and A. E. Sabin (2002). Neogene evolution of the Indian Wells Valley, east-central California, in *Geologic Evolution of the Central Mojave Desert and Southern Basin and Range*, A. F. Glazner, J. D. Walker, and J. M. Bartley (Editors), Geol. Soc. Am. Memoir, Vol. **195,** 199–228.

Pluhar, C. J. (2003). Paleomagnetic and Geochemical applications to tectonics and quaternary geology: studies at Coso Volcanic Field, California and the Channeled Scabland, Washington, *Ph.D. Thesis*, University of California at Santa Cruz, 141 pp.

Pluhar, C. J., R. S. Coe, D. E. Sampson, M. G. Glen, F. C. Monastero, and S. B. Tanner (2005). Lava fingerprinting using paleomagnetism and innovative X-ray fluorescence spectroscopy: a case study from the Coso volcanic field, California, *Geochem. Geophys. Geosystems* **6,** Q04001, doi 10.1029/2004GC000707.

Pujol, J. (2009). Tutorial on rotations in the theories of finite deformation and micropolar (Cosserat) elasticity, *Bull. Seismol. Soc. Am.* **99,** no. 2B, 1011–1027.

Randall, M. J. (1971). Elastic multipole theory and seismic moment, *Bull. Seismol. Soc. Am.* **61,** 1321–1326.

Sipkin, S. A. (1986). Interpretation of non-double-couple earthquake mechanisms derived from moment tensor inversion, *J. Geophys. Res.* **91,** no. B1, 531–547.

Sowers, J. M., J. R. Unruh, W. R. Lettis, and T. D. Rubin (1994). Relationship of the Kickapoo fault to the Johnson Valley and Homestead Valley faults, San Bernardino County, California, *Bull. Seismol. Soc. Am.* **84,** 528–536.

Takeo, M. (2006). Ground rotational motions recorded in near-source region of earthquakes, in *Earthquake Source Asymmetry, Structural Media and Rotational Effects*, R. Teisseyre, M. Takeo, and E. Majewski (Editors), Springer, Berlin, 157–167.

Teisseyre, R. (1973). Earthquake processes in a micromorphic continuum, *Pure Appl. Geophys.* **102,** 15–28.

Teisseyre, R. (1974). Symmetric micromorphic continuum: wave propagation, point source solutions and some applications to earthquake processes, in *Continuum Mechanics Aspects of Geodynamics and Rock Fracture Mechanics*, P. Thoft-Christensen (Editor), Riedel, Dordrecht, 201–244.

Teisseyre, R., and W. Boratyński (2006). Deviations from symmetry and elasticity: asymmetric continuum mechanics, in *Earthquake Source Asymmetry, Structural Media and Rotational Effects*, R. Teisseyre, M. Takeo, and E. Majewski (Editors), Springer, Berlin, 31–41.

Teisseyre, R., and J. T. Kozák (2006). Sources of rotation and twist motion, in *Earthquake Source Asymmetry, Structural Media and Rotational Effects*, R. Teisseyre, M. Takeo, and E. Majewski (Editors), Springer, Berlin, 11–23.

Teisseyre, R., M. Takeo, and E. Majewski (Editors) (2006). *Earthquake Source Asymmetry, Structural Media and Rotational Effects*, Springer, Berlin, 582 pp.

Truesdell, C., and R. A. Toupin (1960). The classical field theories, in *Encyclopedia of Physics, Volume III/1: Principles of Classical Mechanics and Field Theory*, S. Flügge (Editor), Springer, Berlin, 226–793.

Twiss, R. J., and J. R. Unruh (1998). Analysis of fault-slip inversions: do they constrain stress or strain rate?, *J. Geophys. Res.* **103,** no. B6, 12,205–12,222.

Twiss, R. J., and J. R. Unruh (2007). Structure, deformation, and strength of the Loma Prieta fault, northern California, USA, as inferred from the 1989–1990 Loma Prieta aftershock sequence, *Geol. Soc. Am. Bull.* **119,** no. 9, 1079–1106.

Twiss, R. J., G. M. Protzman, and S. D. Hurst (1991). Theory of slickenline patterns based on the velocity gradient tensor and microrotation, *Tectonicphysics* **186,** 215–239.

Twiss, R. J., B. J. Souter, and J. R. Unruh (1993). The effect of block rotations on the averaged micropolar moment tensor and patterns of seismic *P* and *T* axes, *J. Geophys. Res.* **98,** 645–674.

Unruh, J. R., R. J. Twiss, and E. Hauksson (1996). Seismogenic deformation field in the Mojave block and implications for tectonics of the eastern California shear zone, *J. Geophys. Res.* **101,** no. B4, 8335–8361.

Appendix A

The Kronecker Delta for a Volume Average

We show by induction from a two-dimensional model of a granular material composed of hexagonal blocks (Figs. 1 and A1), that the Kronecker delta can be defined as an aver-

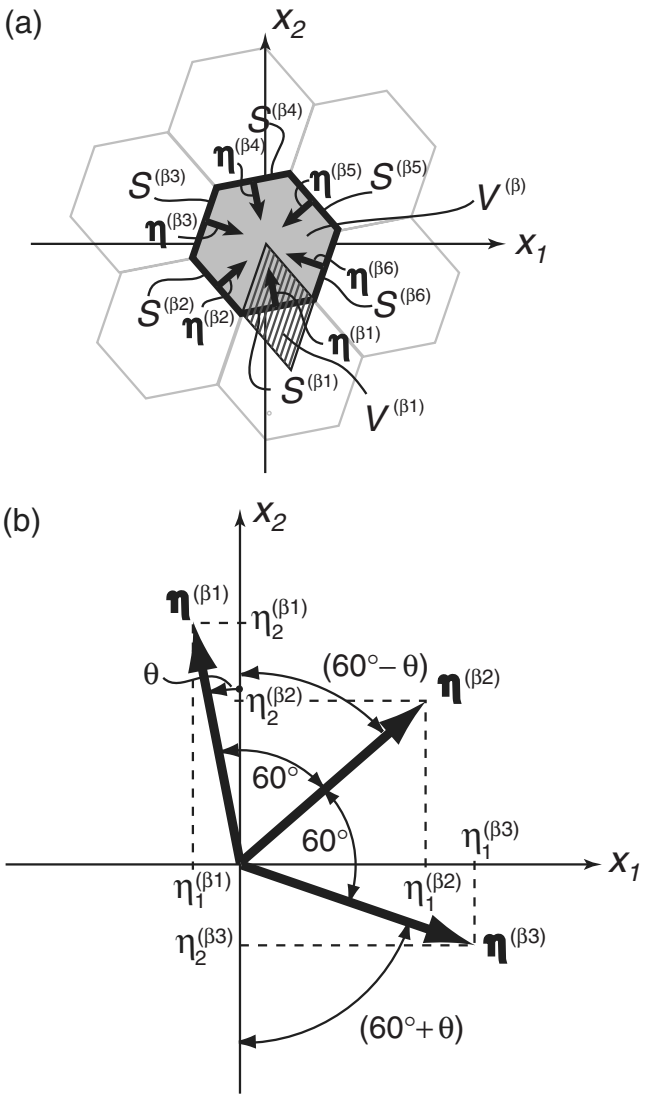

Figure A1. Geometry of a block in an idealized granular material used for defining a volume average over many blocks. (a) The βth block in the granular material, which has a volume $V^{(\beta)}$, is shaded gray. The six surfaces with their inward unit normals are each labeled $S^{(\beta\gamma)}$ and $\boldsymbol{\eta}^{(\beta\gamma)}$, respectively, for $\gamma = 1{:}6$. The volume associated with each shear surface is similar to the one that is diagonally ruled and labeled $V^{(\beta1)}$. (b) The inward unit normals $\boldsymbol{\eta}^{(\beta\gamma)}$ and their components in the common coordinate system $\eta_k^{(\beta\gamma)}$ for three of the surfaces ($\gamma = 1{:}3$) of the βth block plotted from a common origin. The angles show the orientations of these vectors relative to each other and to the common coordinates.

age over a volume $\mathcal{V}$ that is large compared with the block size of the granular material by

$$\delta_{kl} = \frac{1}{\mathcal{V}} \sum_{\alpha=1}^{N} \eta_k^{(\alpha)} \eta_l^{(\alpha)} V^{(\alpha)}, \tag{A1}$$

where $\eta_k^{(\alpha)}$ is the unit normal to the αth surface and $V^{(\alpha)}$ is the volume associated with the αth surface (Fig. A1). We assume the sum is over all the surfaces of all the blocks in the averaging volume $\mathcal{V}$.

Figure A1 shows the geometry of one of the two-dimensional hexagonal blocks that make up the model granular material. The blocks are numbered in some convenient system $\beta = 1{:}B$, and the surfaces on each hexagonal block are numbered $\gamma = 1{:}6$. Thus, the total number of surfaces is given by

$$N = \frac{1}{2} 6B = 3B, \tag{A2}$$

where the factor of a half is required because, in summing the number of surfaces over each of the blocks, each surface is counted twice.

If there are B blocks in the domain over which we are taking the volume average, then the volume of the βth block $V^{(\beta)}$ and the total volume of the domain $\mathcal{V}$ are given in terms of the volume associated with the γth surface of the βth block $V^{(\beta\gamma)}$ by, respectively,

$$V^{(\beta)} = \frac{1}{2} \sum_{\gamma=1}^{6} V^{(\beta\gamma)}, \qquad \mathcal{V} = \sum_{\beta=1}^{B} V^{(\beta)} = \frac{1}{2} \sum_{\beta=1}^{B} \sum_{\gamma=1}^{6} V^{(\beta\gamma)}, \tag{A3}$$

where in the first equation the factor of a half must be introduced, because the volume associated with each surface is twice that contained in the βth block (Fig. A1).

For the two-dimensional model in Figure A1, we see that $V^{(\beta\gamma)}$ is the same for all γ in the βth block, so arbitrarily setting $\gamma = 1$ in equation (A3) we have

$$V^{(\beta)} = \frac{1}{2} (6V^{(\beta 1)}) = 3V^{(\beta 1)}. \tag{A4}$$

From Figure A1 we also see that the inward-pointing unit normals to the surfaces of the block have the components

$$\begin{aligned}
\eta_k^{(1)} &= [-\sin\theta, \cos\theta], \\
\eta_k^{(2)} &= [\sin(60-\theta), \cos(60-\theta)], \\
\eta_k^{(3)} &= [\sin(60+\theta), -\cos(60+\theta)], \\
\eta_k^{(4)} &= [\sin\theta, -\cos\theta], \\
\eta_k^{(5)} &= [-\sin(60-\theta), -\cos(60-\theta)], \\
\eta_k^{(6)} &= [-\sin(60+\theta), \cos(60+\theta)].
\end{aligned} \tag{A5}$$

We define A_{kl} to be the right-hand side of equation (A1), and we show that it is equal to the Kronecker delta:

$$A_{kl} \equiv \frac{1}{\mathcal{V}} \sum_{\alpha=1}^{N} \eta_k^{(\alpha)} \eta_l^{(\alpha)} V^{(\alpha)} = \frac{1}{\mathcal{V}} \sum_{\beta=1}^{B} \sum_{\gamma=1}^{6} \eta_k^{(\beta\gamma)} \eta_l^{(\beta\gamma)} V^{(\beta\gamma)}. \tag{A6}$$

We divide the second summation into two summations over the first three and second three surfaces of the block:

$$A_{kl} = \frac{1}{\mathcal{V}} \sum_{\beta=1}^{B} \left[\sum_{\gamma=1}^{3} \eta_k^{(\beta\gamma)} \eta_l^{(\beta\gamma)} V^{(\beta\gamma)} + \sum_{\gamma=4}^{6} \eta_k^{(\beta\gamma)} \eta_l^{(\beta\gamma)} V^{(\beta\gamma)} \right]. \tag{A7}$$

The symmetry of the model (Fig. A1) allows us to consider just the summation over $\gamma = 1{:}3$ on the right-hand side of equation (A7) because the summation over $\gamma = 4{:}6$ will give the same result.

Introducing the components of the unit normal vectors given by equation (A5) into equation (A7), we can calculate the values of the six components to prove that A_{kl} is the Kronecker delta. For the first component with $(kl) = (11)$, we have

$$A_{11} = \frac{1}{\mathcal{V}} \sum_{\beta=1}^{B} \left[\sum_{\gamma=1}^{3} \eta_1^{(\beta\gamma)} \eta_1^{(\beta\gamma)} V^{(\beta\gamma)} + \sum_{\gamma=4}^{6} \eta_1^{(\beta\gamma)} \eta_1^{(\beta\gamma)} V^{(\beta\gamma)} \right], \tag{A8}$$

$$A_{11} = \frac{1}{\mathcal{V}} \sum_{\beta=1}^{B} \left\{ [\sin^2\theta + \sin^2(60-\theta) + \sin^2(60+\theta)] V^{(\beta 1)} + \sum_{\gamma=4}^{6} \eta_1^{(\beta\gamma)} \eta_1^{(\beta\gamma)} V^{\beta\gamma} \right\}. \tag{A9}$$

Introducing the standard trigonometric relations for the sine of the sum and difference of two angles and then doing some algebra, we find the dependence on θ drops out, leaving

$$A_{11} = \frac{1}{\mathcal{V}} \sum_{\beta=1}^{B} \left[\frac{3}{2} V^{(\beta 1)} + \sum_{\gamma=4}^{6} \eta_1^{(\beta\gamma)} \eta_1^{(\beta\gamma)} V^{(\beta\gamma)} \right]. \tag{A10}$$

By the symmetry of the geometry in Figure A1, we can substitute for the summation in equation (A10)

$$A_{11} = \frac{1}{\mathcal{V}} \sum_{\beta=1}^{B} \left[\frac{3}{2} V^{(\beta 1)} + \frac{3}{2} V^{(\beta 1)} \right] = \frac{1}{\mathcal{V}} \sum_{\beta=1}^{B} 3V^{(\beta 1)}. \tag{A11}$$

Using equation (A4) and then equation (A3), we find

$$A_{11} = 1. \tag{A12}$$

For the off-diagonal component with $(kl) = (12)$, we have

$$A_{12} = \frac{1}{\mathcal{V}} \sum_{\beta=1}^{B} \left[\sum_{\gamma=1}^{3} \eta_1^{(\beta\gamma)} \eta_2^{(\beta\gamma)} V^{(\beta\gamma)} + \sum_{\gamma=4}^{6} \eta_1^{(\beta\gamma)} \eta_2^{(\beta\gamma)} V^{(\beta\gamma)} \right], \tag{A13}$$

$$A_{12} = \frac{1}{\mathcal{V}} \sum_{\beta=1}^{B} \Big\{ \{[-\sin\theta\cos\theta] + [\sin(60-\theta)\cos(60-\theta)] - [\sin(60+\theta)\cos(60+\theta)]\} V^{(\beta 1)} + \sum_{\gamma=4}^{6} \eta_1^{(\beta\gamma)} \eta_2^{(\beta\gamma)} V^{(\beta\gamma)} \Big\}. \tag{A14}$$

Again after substituting the trigonometric relations for the sine and cosine of the sum and difference of two angles (and doing some algebra), we find the dependence on θ drops out, leaving

$$A_{12} = \frac{1}{\mathcal{V}} \sum_{\beta=1}^{B} \left[0 + \sum_{\gamma=4}^{6} \eta_1^{(\beta\gamma)} \eta_2^{(\beta\gamma)} V^{(\beta\gamma)} \right].$$

Applying the symmetry in the geometry of the block and then the symmetry of A_{kl}, we get

$$A_{12} = \frac{1}{\mathcal{V}} \{0 + 0\}, \qquad A_{12} = A_{21} = 0. \tag{A15}$$

Finally, we evaluate the term for which $(kl) = (22)$:

$$A_{22} = \frac{1}{\mathcal{V}} \sum_{\beta=1}^{B} \left[\sum_{\gamma=1}^{3} \eta_2^{(\beta\gamma)} \eta_2^{(\beta\gamma)} V^{(\beta\gamma)} + \sum_{\gamma=4}^{6} \eta_2^{(\beta\gamma)} \eta_2^{(\beta\gamma)} V^{(\beta\gamma)} \right],$$

$$A_{22} = \frac{1}{\mathcal{V}} \sum_{\beta=1}^{B} \Big\{ [\cos^2\theta + \cos^2(60-\theta) + \cos^2(60+\theta)] V^{(\beta 1)} + \sum_{\gamma=4}^{6} \eta_2^{(\beta\gamma)} \eta_2^{(\beta\gamma)} V^{(\beta\gamma)} \Big\}.$$

Using the same procedures as before, we find

$$A_{22} = \frac{1}{\mathcal{V}} \sum_{\beta=1}^{B} \left\{ \left[\frac{3}{2} \right] V^{(\beta 1)} + \sum_{\gamma=4}^{6} \eta_2^{(\beta\gamma)} \eta_2^{(\beta\gamma)} V^{(\beta\gamma)} \right\}. \tag{A16}$$

Again using the symmetry of the model geometry with equation (A5), we see that the summation over $\gamma = 4{:}6$ is identical to that for $\gamma = 1{:}3$. Then, using equation (A4) we get

$$A_{22} = \frac{1}{\mathcal{V}} \sum_{\beta=1}^{B} \left[\frac{3}{2} V^{(\beta 1)} + \frac{3}{2} V^{(\beta 1)} \right] = \frac{1}{\mathcal{V}} \sum_{\beta=1}^{B} 3V^{(\beta 1)} = \frac{1}{\mathcal{V}} \sum_{\beta=1}^{B} V^{(\beta)}, \tag{A17}$$

$$A_{22} = 1. \tag{A18}$$

Thus, from equations (A12), (A15), and (A18) we see that equation (6) becomes

$$A_{kl} = \frac{1}{\mathcal{V}} \sum_{\alpha=1}^{N} \eta_k^{(\alpha)} \eta_l^{(\alpha)} V^{(\alpha)} = \frac{1}{\mathcal{V}} \sum_{\beta=1}^{B} \sum_{\gamma=1}^{6} \eta_k^{(\beta\gamma)} \eta_l^{(\beta\gamma)} V^{(\beta\gamma)} = \begin{bmatrix} 1 & 0 \\ 0 & 1 \end{bmatrix}, \tag{A19}$$

$$A_{kl} = \delta_{kl}. \tag{A20}$$

Q.E.D.

Thus, we have proven equation (A1) for the particular geometry of Figure A1. This result also applies in the special case for which there is only one hexagonal block ($B = 1$), and the summation over $\gamma = 1{:}L$ is over all six surfaces that bound that block. By induction, we infer that this is a general result for a block of any geometry if the summation occurs over all surfaces that define a closed surface for the block. Thus, we conclude

$$\delta_{kl} \equiv \frac{1}{V^{(\beta)}} \sum_{\gamma=1}^{L} \eta_k^{(\beta\gamma)} \eta_l^{(\beta\gamma)} V^{(\beta\gamma)}. \tag{A21}$$

In general, we expect that for any given record of a series of earthquakes, the N surfaces on which slip events have occurred will not include all the surfaces of any single block, nor will they include all the surfaces of all the blocks in the domain. We assume, however, that if N is sufficiently large, these surfaces will have a distribution of orientations that on the average will be similar to that for the surfaces bounding any given block. Thus, for sufficiently large N, equation (A1) would still hold. Given sufficient time, ultimately slip must occur on all surfaces of each block in order to accommodate the rotation of the block.

Appendix B

Antisymmetry of the Averaged Microrotation Tensor

We want to show that when the local slip vectors due to block rotations are averaged over all the surfaces of a block, the result is an antisymmetric averaged rotation tensor. We illustrate this result in two dimensions using one of the hex-

agonal blocks (see Fig. A1), which rotates about the axis normal to the plane of the two-dimensional block.

We modify the notation by which we identify an individual surface (α) by specifying the number β of a specific block in the granular material and the number γ of the surface of that block, so a specific surface becomes designated by its block number and surface number ($\beta\gamma$). Thus, from equation (68) the microrotation is the average of the block rotations defined for each surface:

$$\mathcal{R}_{ij} \equiv \frac{1}{\mathcal{V}} \sum_{\alpha=1}^{N} R_{im}^{(\alpha)} \eta_m^{(\alpha)} \eta_j^{(\alpha)} V^{(\alpha)} = \frac{1}{\mathcal{V}} \sum_{\beta=1}^{B} \sum_{\gamma=1}^{6} R_{im}^{(\beta\gamma)} \eta_m^{(\beta\gamma)} \eta_j^{(\beta\gamma)} V^{(\beta\gamma)}. \quad \text{(B1)}$$

Because we assume each block to be rigid, the rotation for all surfaces of a given block must be the same. Thus,

$$R_{ij}^{(\beta\gamma)} = R_{ij}^{(\beta)} \quad \text{for all } \gamma, \quad \text{(B2)}$$

whereby equation (B1) becomes

$$\mathcal{R}_{ij} \equiv \frac{1}{\mathcal{V}} \sum_{\beta=1}^{B} R_{im}^{(\beta)} \left[\sum_{\gamma=1}^{6} \eta_m^{(\beta\gamma)} \eta_j^{(\beta\gamma)} V^{(\beta\gamma)} \right]. \quad \text{(B3)}$$

For the summation on all surfaces of the βth block, which is the term within the brackets in equation (B3), we use equation (A21) to find

$$\mathcal{R}_{ij} \equiv \frac{1}{\mathcal{V}} \sum_{\beta=1}^{B} R_{im}^{(\beta)} \{ V^{(\beta)} \delta_{mj} \} = \frac{1}{\mathcal{V}} \sum_{\beta=1}^{B} R_{ij}^{(\beta)} V^{(\beta)}. \quad \text{(B4)}$$

However, from equation (60) we see that the microrotation tensor is antisymmetric for any given surface, and it is the same for the rigid block of which that surface is a part. Equations (B4) and (60), therefore, imply

$$\mathcal{R}_{ij} = \frac{1}{\mathcal{V}} \sum_{\beta=1}^{B} R_{ij}^{(\beta)} V^{(\beta)} = -\frac{1}{\mathcal{V}} \sum_{\beta=1}^{B} R_{ji}^{(\beta)} V^{(\beta)} = -\mathcal{R}_{ji}. \quad \text{(B5)}$$

Thus, the instantaneous microrotation tensor is antisymmetric.

Department of Geology
University of California, Davis
Davis, California 95616
twiss@geology.ucdavis.edu

Manuscript received 19 May 2008